On the Mechanical Behaviour of Test Specimens for Wood-Adhesive Bonds

Serrano, Erik

2002

Document Version:
Publisher's PDF, also known as Version of record

LUND UNIVERSITY

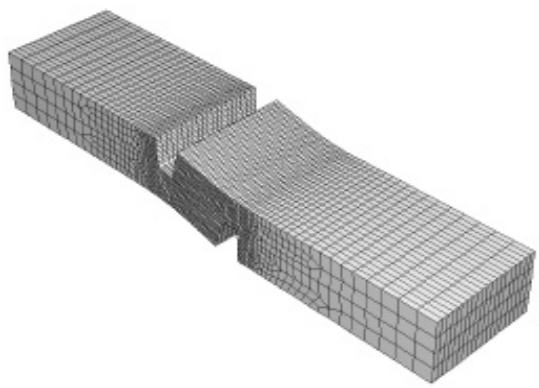

ON THE MECHANICAL BEHAVIOUR OF TEST SPECIMENS FOR WOOD-ADHESIVE BONDS

ERIK SERRANO

Structural Mechanics

Structural Mechanics

ISRN LUTVDG/TVSM--02/3063--SE (1-73)
ISSN 0281-6679

ON THE MECHANICAL BEHAVIOUR OF TEST SPECIMENS FOR WOOD-ADHESIVE BONDS

ERIK SERRANO

Printed by KFS I Lund AB, Lund, Sweden, October, 2002.

For information, address:
Division of Structural Mechanics, LTH, Lund University, Box 118, SE-221 00 Lund, Sweden.
Homepage: http://www.byggmek.lth.se

Preface

This report presents the results from a numerical finite element study on the mechanical behaviour of wood adhesive test specimens. The work was initiated and financed by the Swedish National Testing and Research Institute, Borås (SP).

I would like to express my gratitude to Mr. Björn Källander and Dr. Charlotte Bengtsson at building technology, wood materials, SP, for making it possible for me to keep working with my favourite subjects: wood-adhesive bonds, non-linear fracture mechanics and finite elements.

Lund, September 2002

Erik Serrano

Abstract

This investigation relates to the mechanical behaviour of some different test specimens for wood-adhesive bond tests. The main objective is to investigate the sensitivity of the various test methods to geometrical imperfections, bound to be present in any real-life test situation. Finite element analyses were performed with a nonlinear material description for the behaviour of the bond line. The material parameters used for the wood material were chosen in order to represent an estimated average of Swedish beech, and the bond line parameters were chosen to represent three different adhesive types, ranging from ductile to brittle. The specimen types investigated correspond to the standards according to ASTM-D4680, ASTM-D905 and EN302-1. A modified version of the specimen as specified by ASTM-D3535 was also investigated.

The results from the simulations show that the mechanical behaviour in terms of estimated bond line strength, i.e. in terms of load bearing capacity of the joint is highly dependent on both the specimen type used *and* the adhesive properties. As an example, it was shown that the ASTM-D905 specimen was not able to rank the adhesives in terms of local bond line strength. Instead the bond line with highest local strength was ranked as being weaker than a more ductile adhesive having a lesser local strength.

Another outcome is that the sensitivity to geometrical imperfections and erroneous load application is also highly dependent on specimen *and* adhesive type.

The ASTM-D3535-alike specimen is manufactured from 14 smaller pieces of wood, forming a complex-shaped specimen with 12 active bond lines. This specimen was found to give good predictions of local strength for the case when all bond lines were assigned the same strength value. This is mainly thanks to the relatively short overlap lengths of the individual bond lines. However, in a real testing situation, there is bound to be a variation in bond strength within each bond line and between bond lines. Therefore, a further investigation was undertaken by changing the local strength of one of the 12 active bond lines. The results show that this multiple bond line specimen gives an estimate of the *weakest* of the 12 bond lines as an estimate of local strength. Therefore, results obtained with this test method cannot be compared with results obtained from single bond line specimens, at least not without statistical considerations.

Table of Contents

1 Introduction

1.1 Background and Aim

Test methods for testing wood adhesives for creep and creep rupture are being discussed in a working group of CEN/TC193/SC1. This is aimed at developing a test method or set of test methods by which new adhesives can be evaluated. The interest so far has been focused on 2 methods, ASTM D 3535-92 and ASTM D 4680-92. Some attention has also been on the EN302-1 specimen for thin bond lines. In this report, these specimens are all investigated, together with the ASTM D905 shear test specimen.

The work presented in this report was performed on behalf of the Swedish National Testing and Research Institute, in an attempt to offer a detailed background for decision-making.

1.2 Specimen Preparation, Test Methods and Rational Models

Testing of wood-adhesive bonds can have many purposes, and consequently a number of test methods are available. Two different methods in terms of sample preparation are possible: a) to cut out a specimen from a "real structure" and b) to manufacture a "laboratory" specimen. Each of these two methods has its respective advantages and disadvantages. While for most cases it is difficult, not to say impossible, to cut out a test specimen from a larger structure without inflicting any damage to the specimen, it is still an appealing approach, due to the fact that the formation of the bond line in question has taken place under "real-life" conditions. Another disadvantage of the "in-situ"-method, apart from the difficulty of cutting it, is that for some situations it may result in specimens not suited for "simple" evaluation of the test results. Here, simple means well-defined states of stresses or strains. The laboratory specimen approach is the most commonly used, its main advantages being the possibility to obtain a well-defined geometry and, hopefully a well defined loading and state of stress.

In order to obtain fundamental knowledge of the mechanical behaviour of wood-adhesive joints it is necessary to use an approach, based on rational arguments. The term "rational arguments" means arguments based on a commonly accepted theory, as for instance the theory of strength of materials. The use of such a theory results in an explanatory approach, and can be seen as the opposite of a completely non-explanatory, empirical approach or "theory".

Many tests performed in practice are made to evaluate e.g. the quality of the adhesive or the joint manufacturing and are performed as comparative studies, i.e. a study aiming at concluding if a certain adhesive system behaves better or poorer than another one. The question arises if for such comparative studies, the only conclusion that can be drawn is that a certain adhesive system performs better or worse only in terms of fulfilling the criteria set up by the method itself.

1.3 Factors Affecting Joint Strength

The load bearing capacity of an adhesive joint depends on many parameters. For one-dimensional states of stress, the *normalised strength* is the ratio of the "strength of the joint" to the "local strength of the bond line", where the joint strength is equal to e.g. the maximum load divided by the fracture area. This dimensionless ratio, denoted τ^*, has an upper bound of 1.0, which can be obtained for an ideal plastic adhesive. For other adhesives than the ideal plastic ones, i.e. any adhesive encountered in real-life, τ^* is less than 1.0. Thus, the deviation from this value is an indication of the accuracy of the present test method to measure the local strength of the bond line. Consequently, *if* local

strength is what one wishes to measure, then the value of τ^* should be close to 1.0. According to the theory of nonlinear fracture mechanics, for a given geometrical shape of the specimen and for the case that material parameters are all known for the current environmental conditions and any possible history of loading and environmental effects, the following parameters govern the normalised strength of the joint: local strength, bond line fracture energy, adherend material stiffness, absolute size of the joint and shape of the stress-slip relation of the bond line.

1.4 Scope and Limitations

The theory used in this work was originally developed for analysing thin wood-adhesive bond lines subjected to short-term static and monotonic loading at constant climatic conditions. This is in contrast with typical applications found in real-life, which often include long term loading and varying loading conditions. However, it is still of great value to be able to analyse the basic behaviour of complex loading and geometry conditions, such as can occur in the test situations considered here. Work similar to the work presented here was performed for two of the current specimens, in Wernersson (1994). However, that investigation was performed for one adhesive type only, and assuming plane stress conditions. Here a more complete investigation, including a range of adhesive properties and 3D simulations has been performed. For one of the specimens, however only 2D simulations were possible to perform. Hopefully this work should at least represent a starting point for fruitful discussions regarding the choice of a proper future test method.

2 Bond Line Model and Material Parameters

2.1 General Remarks

An adhesive *joint* is defined as a connection, composed by the bonding agent (the adhesive or glue) and the adherends (the wood material). These two materials, when put together and allowed to interact (penetration into the wood and curing of the adhesive) can form a bond line. In the present study, a *bond line* is defined as the region between the two solid adherends. The bond line is often subdivided into the adhesive bulk and two interface regions, one in the vicinity of each adherend. Physically, these interface regions have a small but finite thickness, related to the penetration of the adhesive into the wood and to the length of the wood fibres on the adherend surface.

Since adhesive bonds are exposed to compressive stresses during curing, resulting in the adhesive penetrating the wood, it seems natural to consider the interface region being a part of the adherend rather than being a part of the adhesive bulk. Normally, in a design situation, the nominal thickness of the bond line, defined as the distance between the adherend surfaces after curing, is known. However, little or no information is available regarding the penetration of the adhesive into the wood. Therefore, from a practical point of view, it is convenient to define the adhesive bulk thickness as being equal to the nominal thickness of the bond line, and assume the interface region to have a zero thickness. This is the approach taken in this study, and the bond line model is assumed to account for the total response of the bulk *and* the interface regions. The definitions of the bond line components together with some main notations are given in Figure 1.

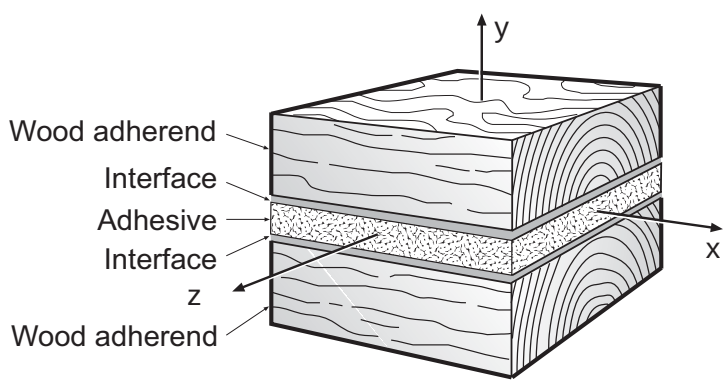

Figure 1. Components of a wood adhesive bond line and notation used for local bond line coordinate system.

The bond line model used is based on a nonlinear fracture mechanics model originally developed by Wernersson (1994) and also used in previous studies by Serrano (2000). The model is implemented in a commercial finite element software as a user-defined material. The bond line material is applied to a single bond line element and thus the approach used is that of a crack band model. The current version of the material model allows for three-dimensional structures to be analysed, taking into account the softening of the adhesive layer for the two in-plane shear stress components and the normal stress perpendicular to the bond layer. The three remaining stress components (two in-plane normal stresses and out of plane shear stress) are assumed to follow a linear elastic behaviour.

The current material model can be described as strain- or fracture softening. This means that after maximum stress has been reached, the bond line has still load-bearing capacity left, but this capacity diminishes as the deformation, or slip across the bond line, increases. A schematic of this type of response is depicted in Figure 2

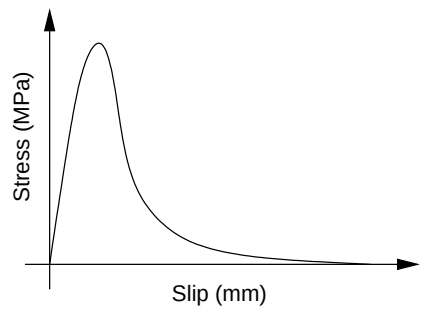

Figure 2. Uniaxial response of a softening material.

The model is not formulated in terms of plasticity or damage, but is implemented as being nonlinear elastic, and is therefore not suitable for cyclic loading or if considerable unloading occurs.

The material model parameters needed are the uniaxial stress-slip curves, including softening for the three active stress components, cf. Figure 2. Also the coupling, or interaction between the behaviour in different loading directions must be defined. This interaction is defined through exponents, describing the initial failure for multi-axial states of stress. Denoting the uniaxial strengths of the bond line with f_{v1}, f_{v2} and f_t for the two shear strengths and the peel stress respectively, the present model uses the following type of relation:

$$\left(\frac{\tau_{xz}}{f_{v1}}\right)^{m} + \left(\frac{\tau_{xy}}{f_{v2}}\right)^{n} + \left(\frac{\sigma_{y}}{f_{t}}\right)^{p} = 1.0 \qquad (1)$$

The model allows for different values of the coupling powers *m, n* and *p* to be used. For more details of the material model see Wernersson (1994) and Serrano (2000).

In order not to be limited to use a special kind of smooth function to represent the uniaxial softening response, the bond line model is based on piecewise linear relations. This is the simplest but yet most general approach to fit arbitrary curve shapes recorded in tests.

The bond line response can be visualised in terms of a stress surface in displacement space e.g. τ_{xy} versus the shear slip and normal opening displacement across the bond line. Such a surface is shown in Figure 3 for the case of m=n=2, which has shown to give a reasonable fit for the strength of a PR adhesive. Although the current material model is expressed in terms of stress versus slip across the bond line, it is often convenient to express the material response in terms of stress versus strain, by assuming a uniform strain across the bond line thickness. In this way a material length is introduced in the constitutive relations.

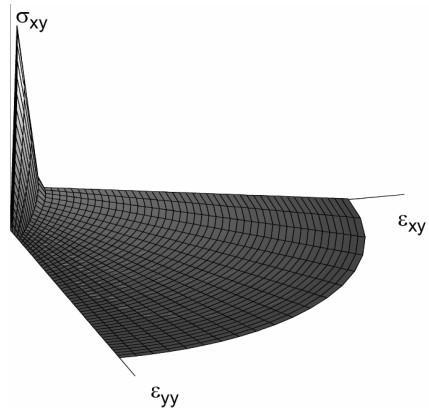

Figure 3. Shear stress versus shear and normal strain (slip).

2.2 Bond Line and Joint Parameters

The input data used for the bond line material model are estimates using the experience from previous investigations by Wernersson (1994) and Serrano (2000). Three sets of parameters, ranging from brittle to ductile have been used. These sets are thought to be representative for adhesive used in different wood applications. The three adhesive types will be referred to as (from brittle to ductile): PRF, PUR and PVA, denoting Phenol-resorcinol-formaldehyde, Polyurethane and Polyvinyl acetate-based formulations respectively.

The term ductility is sometimes used as being equivalent to the fracture energy. Here instead we will use a measure of the ductility based on both bond line strength *and* fracture energy. This is inspired by the so-called characteristic length, a ductility measure that has been used for other materials modelled with nonlinear fracture mechanics, such as concrete. The characteristic length, l_{ch} , of a material is defined by:

$$l_{ch} = \frac{EG_f}{f_t^2} \tag{2}$$

where E, is the material stiffness (Young's modulus), G_f is the fracture energy and f_t is the material strength. Following this definition the ductility of a bond line is defined by the ratio G_f/f_t^2 (unit *m/MPa*). Table 1 gives this ductility parameter together with the two most important material properties, the shear strength and shear mode fracture energy of the bond line.

Table 1. Summary of bond line properties for three adhesive types.

Adhesive	Shear strength (MPa)	Shear mode fracture energy (J/m^2)	Ductility, G_f/f_t^2 (m/MPa)
PR	18	1250	3.86
PUR	12	1230	8.54
PVAc	8	2400	37.5

The stress versus slip curves used to define the input for the three adhesive types are shown in Figure 4. The uniaxial curves for peel stress are assumed to be identical for the three adhesives. This is explained by the fact that the behaviour in this loading mode, is more influenced by the adherend properties than it is in shearing mode. As mentioned above, the *material brittleness* can be expressed in terms of its characteristic length, l_{ch}. The *joint brittleness ratio*, denoted ω, is the ratio of the absolute size of the joint to l_{ch} [m], and is thus a dimensionless quantity. Using dimensionless forms in analysing results gives general and valuable information about equivalent quantities in terms of influence on load bearing capacity. For example, since ω is the ratio of absolute size to l_{ch}, the absolute size of the joint has the same impact on joint normalised strength as has the fracture energy.

2.3 Wood

The wood adherends are modelled as being linear elastic and orthotropic. The following material parameters are used throughout this study (*l, r* and *t* denote the longitudinal, radial and tangential directions respectively): E_l=13800, E_r=2200, E_t=1140, G_{lr}=1610, G_{lt}=1060, G_{tr}=640 (*MPa*), ν_{lr}= 0.45, ν_{lt}= 0.52, ν_{rt}= 0.71. These values were taken from Kollmann and Côte (1968) and are according to this reference, valid for a density of 740 kg/m^3 at 10.7% MC.

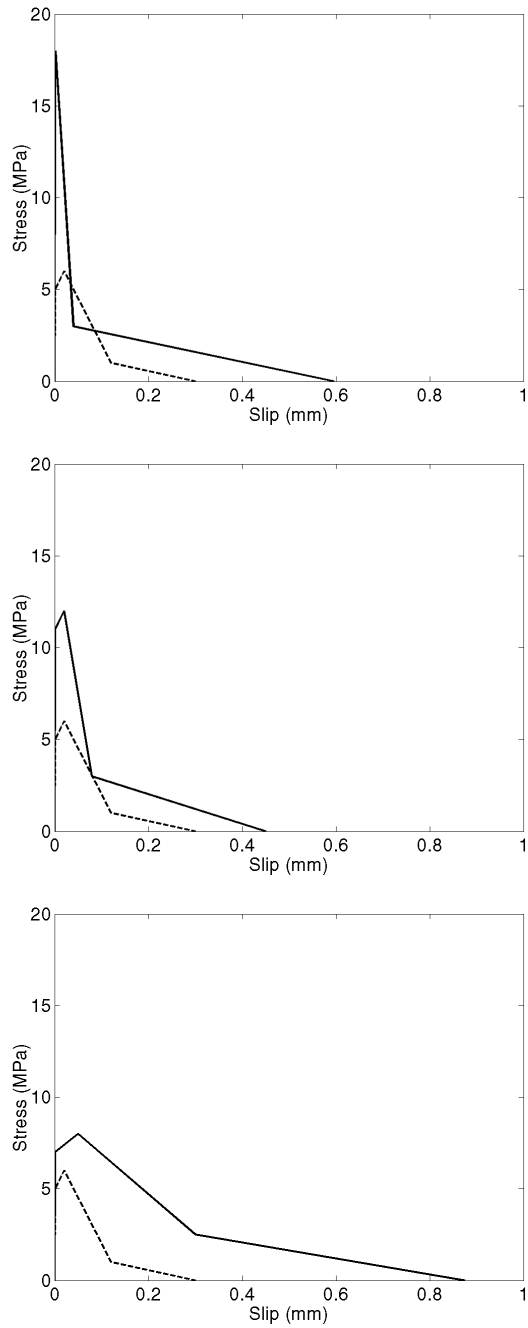

Figure 4. Bond line uniaxial stress-slip curves. From top to bottom: PR, PUR and PVAc. Solid lines correspond to shear stress and dashed lines to normal (peel) stress. The response in shear is assumed to be identical for the two different shear directions.

3 Specimens, FE-models and Simulation Schemes

3.1 General Remarks

A total of four different test specimens were investigated. These correspond to the standards according to ASTM-D4680, ASTM-D905 and EN302-1. A modified version of the ASTM-D3535 was also investigated. Although modified this specimen will be referred to as "ASTM D3535". For all specimen types, three reference simulations were performed using the nominal geometry of the specimen according to specifications in the respective standards. For each of the specimen types a number of different load application errors were simulated by applying the load eccentrically. For the ASTM-D4680 and D905 specimens, the erroneous load application was also achieved by assuming that the specimen geometry deviated from the nominal perfect brick shape. Simulations were also performed in order to investigate the behaviour of the complex-shaped ASTM-D3535 specimen for the case of varying local strength between different bond lines.

The simulations of the D4680, the D905 and the EN302-1 specimens were performed as 3D-simulations. The D3535 specimen was analysed assuming plane strain conditions due to its large size. It has been assumed in all simulations that the shear-tests are performed in the *l-r* direction of the wood. The wood material has for all cases been modelled as an orthotropic material, with its principal directions defined by a rectangular coordinate system.

3.2 ASTM D905

The D905-specimen consists of two wood pieces, which are bonded by a single bond line. The specimen is tested in compression, cf. Figure 5.

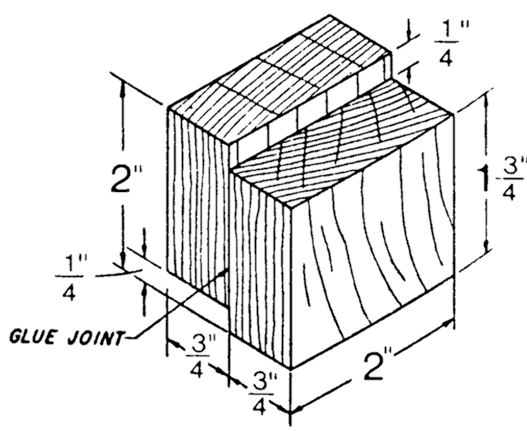

Figure 5. The ASTM-D905 specimen.

The nominal geometry and the geometrical imperfection used is shown in Figure 6. First an investigation of influence the friction between the loading arrangement and the specimen was investigated. Two different coefficients of friction, μ, are tested for each adhesive, μ=0 and 0.3 respectively. This results in 6 simulations. The second changing parameter is the slope of the end face, ϕ. The investigation covers slopes of 1° and 5° for each adhesive. This results in an additional 6 simulations. Another way of simulating a

similar imperfection is to assume the loading of the specimen to be applied at different distances from the bond line, *e* in Figure 6. Here, three additional simulations are made for each adhesive type for *e*=0.5, 2.0 and 4.0 mm respectively. This results in 9 additional simulations, making a total of 21 simulations for this specimen.

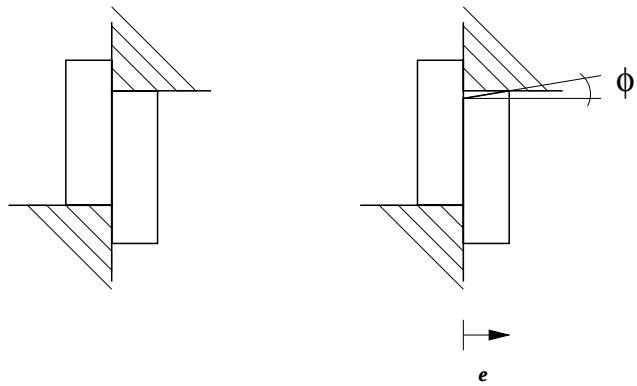

Figure 6. Schematic of ASTM-D905 specimen and suggested geometry imperfection.

The finite element model used is shown in Figure 7. The model consists of approximately 24000 elements, of which 1280 elements define the adhesive layer. The loading is applied by using two rigid surfaces, simulating the steel parts of the test set-up. The wood material directions are defined such that they coincide with the principal directions of the adhesive layer. Consequently, the longitudinal direction of the wood is parallel to the loading direction (direction 2), the radial direction coincides with the normal of the adhesive layer (direction 1) and the tangential direction is perpendicular to both these directions (direction 3). This coincides with what one would obtain for a small specimen cut out from a long distance from the pith of the stem. The adhesive bond line thickness is 0.1 mm and is modelled with a single layer of elements with nonlinear material properties as defined above. Due to the symmetry of the specimen geometry, only half of its width (3-direction) was modelled. This also means that the current model only can be used for load cases that are symmetric with respect to the 1-2-plane (Figure 7).

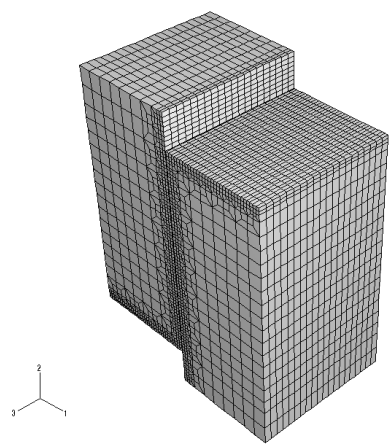

Figure 7. Finite element mesh used in the simulations of the D905 specimen (symmetric half).

The loading is applied by prescribing the displacement of the upper rigid surface. The rigid surfaces are completely fixed in all directions but the loading direction. The applied load and the corresponding mean shear stress in the adhesive layer, is estimated by the reaction force in the 2-axis direction of the lower rigid surface. This means that for the case when friction is involved, the frictional forces are included in the estimate of mean shear stress in the adhesive layer. The rigid surfaces and a close-up of the adhesive layer region are shown in Figure 8, which also shows the eccentric loading.

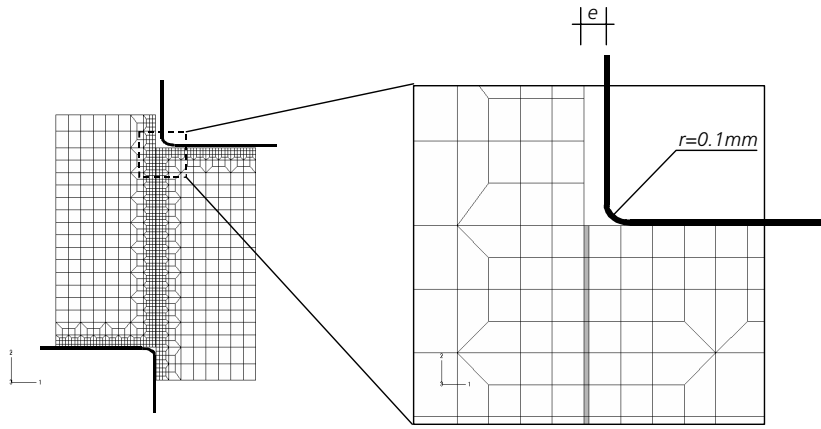

Figure 8. Side-view of FE-model with rigid surfaces (left) and close-up of adhesive layer and rigid surface with filleted corner (right). Different distances e=0, 0.5, 2 and 4 mm were investigated.

The complete simulation scheme is presented in Table 2, and for each type of simulation, three different adhesives were investigated. The adhesives are denoted PRF, PUR and PVA for the brittle, intermediate and ductile types respectively. The adhesive type and simulation number denotes the different simulations. For example "prf01" means simulation type 1 with PRF-adhesive properties (brittle adhesive).

Table 2. Simulation scheme, D905-specimen. Each type is performed for three adhesives.

Simulation type, no.	Eccentricity, e (mm)	Coefficient of friction	Slope of end-face
01	0	0.3	0
02	0.5	0.3	0
03	2	0.3	0
04	4	0.3	0
05	0	0	0
06	0	0.3	1°
07	0	0.3	5°

3.3 ASTM D3535

The D3535-specimen analysed here is a modified version of the one described in the original standard. For simplicity however, the name D3535 will be used. The geometry of the specimen was modelled as close as possible to the geometry used by SP, which means that the bond lines in the specimens were 12.5 mm long and 50 mm wide. The gaps between the individual pieces were 3.2 and 6.4 mm respectively, and thus the individual pieces that build up the test configuration were 28.2 mm (mid pieces) and 31.4 mm (outer pieces). The original ASTM specimen was furthermore altered so that a total of 12 bond lines are tested simultaneously, cf. Figure 9. All bond lines were assumed to be of 0.1 mm thickness. In the simulations, the specimen is loaded in compression by applying forces at the ends of the specimen by means of rigid surfaces. First the influence of eccentric placement of the loading by applying loads at different positions as defined by in Figure 9 was investigated. The rigid surface at the left end was given a prescribed displacement in the x-direction and was prevented from moving in the y-direction. The left-end rigid surface was free to rotate. For every adhesive type eccentricities of 0.5 2 and 4 mm with a coefficient of friction of 0.3 was investigated. Also the influence of applying a centric load but prescribing a small in-plane rotation of the left-end rigid surface was investigated. This results in a loading very similar to the eccentric loading. For all cases investigated, the right-end rigid surface was fixed. A total of 6 loading conditions×3 adhesive types=18 simulations were performed according to Table 3.

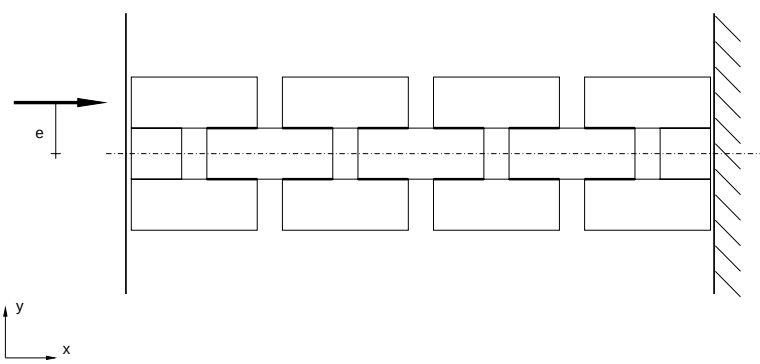

Figure 9. ASTM D3535 specimen with 12 active bond lines (thick lines) in side view. Compressive loading is applied by means of rigid surfaces in contact with the specimen ends.

Table 3. Simulation scheme, D3535-specimen. Each type is performed for three adhesives

Simulation type no.	eccentricity, e (mm)	coefficient of friction	prescribed rotation (rad/mm)
01	0	0.3	0
02	0.5	0.3	0
03	2	0.3	0
04	4	0.3	0
05	0	0.3	0.01
06	0	0.3	0.02

The FE-mesh used in the simulations is shown in Figure 10. Each bond line is modelled with 25 elements (each element is 0.5 mm in length). The model consists of approximately 23000 elements and 24000 nodes, making a total of approximately 48000 degrees of freedom. The wood material is oriented such that the longitudinal direction corresponds to direction 1 and the radial direction corresponds to direction 2.

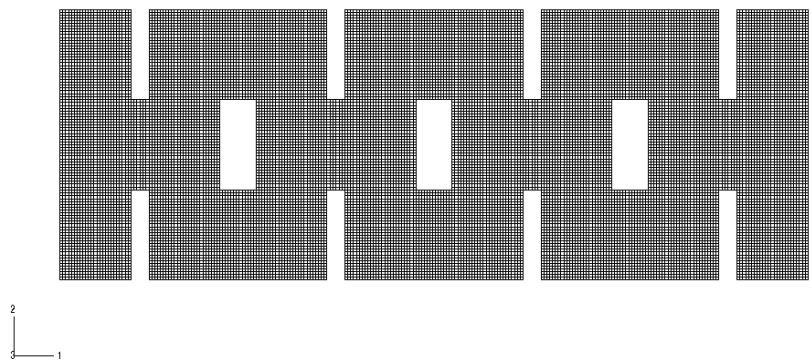

Figure 10. FE-mesh used in the simulations of the ASTM D3535-specimen.

3.4 EN-302-1

The EN-302-specimen is based on a single overlap joint with tensile loading according to the schematic in Figure 11. The forces at the ends are applied by assuming that plane end-sections remain plane. The left end is pinned (free to rotate) and the right end is completely fixed. The free length of the specimen is 85 mm, the length of the adhesive bond line to be tested is 10 mm. Finally, the specimen width, *b,* is 20mm and the thickness, *t,* is 10 mm.

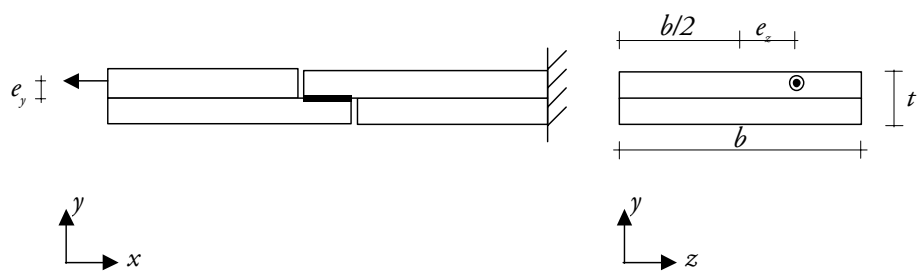

Figure 11. Schematic of the EN-302-1 specimen. Side view (left) and end view (right)

The investigation includes applying the tensile force eccentrically by choosing the eccentricity e_z to be 0, 1, 2 and 4 mm in the width direction and e_y to be 1 and 2 mm in the thickness direction, respectively. A total of 8 eccentricities×3 adhesives=24 simulations were performed, as defined in Table 4.

Table 4. Simulation scheme, EN302-1-specimen. Each type is performed for three adhesives

Simulation type no.	eccentricity, e_z (mm)	eccentricity, e_y (mm)
01	0	0
02	1	0
03	2	0
04	4	0
05	1	1
06	2	1
07	4	1
08	4	2

The FE-mesh used in the simulations is shown in Figure 12. The bond line, o.1 mm in thickness, is modelled with 25 elements in the 1-direction and 20 elements in 3-direction. Each element is thus 0.4×1×0.1 mm^3. The model consists of approximately 23000 elements and 26000 nodes, making a total of approximately 79000 degrees of freedom. The wood material is oriented such that *l*=1, *r*=2 and *t*=3.

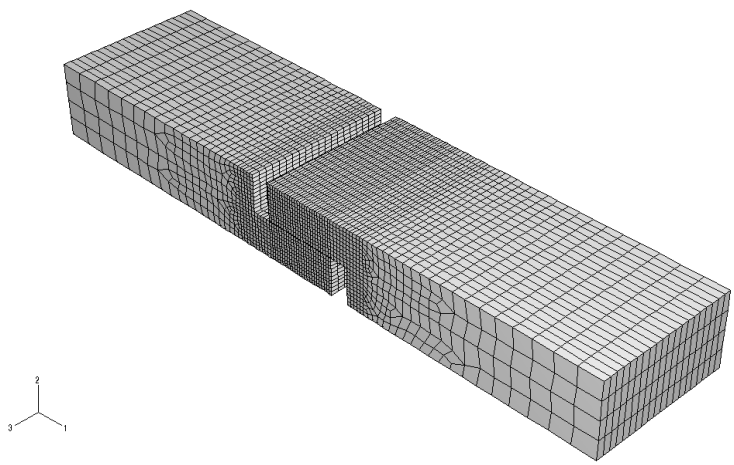

Figure 12. FE-mesh used in the simulations of the EN302-1-specimen.

3.5 ASTM D4680

The D4680 specimen is similar to the D905 specimen block shear specimen built from two wood pieces. However, the D4680 specimen is smaller in size and with different shape, cf. Figure 13.

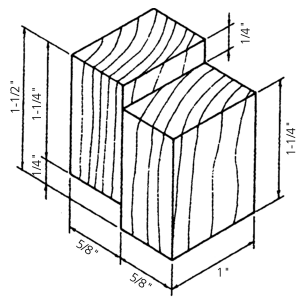

Figure 13. The ASTM-D4680 specimen.

The specimen was simulated using the same loading and boundary conditions as for the D905 specimen. The FE-mesh used for one symmetric half of the specimen is shown in Figure 14. The model consists of approximately 12900 elements of which 640 elements are used for the bond line. The simulations performed for this specimen are summarised in Table 5

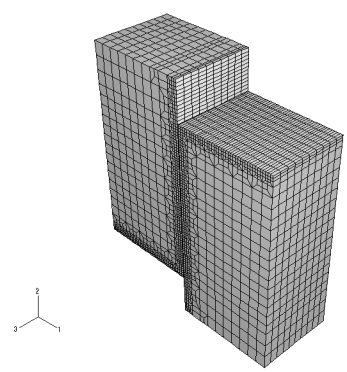

Figure 14. FE-mesh used in the simulations of the D4680 specimen (symmetric half).

Table 5. Simulation scheme, D4680-specimen. Each type is performed for three adhesives.

Simulation type, no.	Eccentricity, e (mm)	Coefficient of friction	Slope of end-face
01	0	0.3	0
02	0.5	0.3	0
03	2	0.3	0
04	4	0.3	0
05	0	0	0
06	0	0.3	1°
07	0	0.3	5°

4 Results

4.1 General Remarks

The results from the above-defined simulations for different adhesive types, geometric imperfections and specimen types are presented shortly below. Detailed results are presented in Appendices A-C for the three specimen types. Here, only typical and the most important conclusions are given. Results are presented as deformation plots, load vs. deformation curves and stress distributions at a linear elastic state and at maximum load. The stress distributions include the shear stresses and the peel stress as determined in the mid-plane of the adhesive layer. For the case of the ASTM-D3535 specimen, the first and second upper bond line (from the left end) is used for presentation of the results.

4.2 ASTM D905

The deformed specimen at maximum load for the cases "prf01" is shown in Figure 15. The deformations are scaled by a factor of 10, for clarity. For this case there is contact between the short vertical sides of the specimen and the loading surfaces.

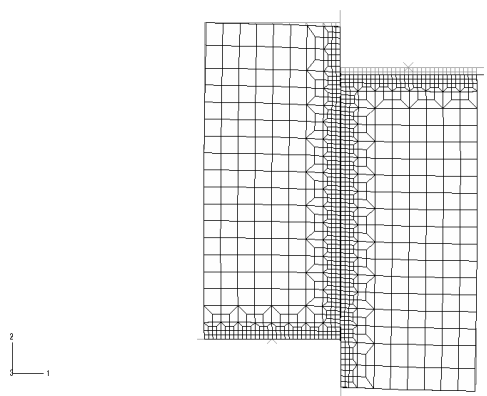

Figure 15. Deformed plot of prf01-specimen. Undeformed plot is superimposed.

The results from the simulations are summarised in Table 6, giving load-bearing capacities and corresponding average shear stress at failure, calculated by dividing the maximum load by the nominal fracture area. Also the average shear stress calculated from the shear stress distribution along the bond line is given. This in an attempt to disregard any influence of frictional forces.

Table 6. Results from simulations of the ASTM905 specimen.

Name	P_{ult} (kN)[1]	τ (MPa)[2]	τ* (-)[2]	τ (MPa)[3]	τ* (-)[3]
PRF01	10.7	11.1	0.61	10.2	0.57
PUR01	11.1	11.5	0.96	10.6	0.88
PVA01	8.22	8.49	1.06	7.80	0.98
PRF02	10.2	10.6	0.58	10.2	0.57
PUR02	10.9	11.3	0.94	10.8	0.90
PVA02	7.90	8.16	1.02	7.8	0.98
PRF03	9.43	9.74	0.54	9.33	0.52
PUR03	10.5	10.8	0.90	10.4	0.86
PVA03	7.93	8.20	1.02	7.82	0.98
PRF04	8.59	8.88	0.49	8.46	0.47
PUR04	9.65	9.98	0.83	9.50	0.79
PVA04	7.86	8.12	1.02	7.71	0.96
PRF05	8.33	8.61	0.48	8.61	0.48
PUR05	9.20	9.51	0.79	9.41	0.78
PVA05	7.30	7.55	0.94	7.47	0.93
PRF06	8.32	8.59	0.48	7.20	0.40
PUR06	9.18	9.49	0.79	7.96	0.66
PVA06	7.70	7.96	0.99	6.59	0.82
PRF07	8.07	8.34	0.46	6.92	0.38
PUR07	8.48	8.76	0.49	7.28	0.40
PVA07	7.44	7.68	0.96	6.35	0.79

Note that the local shear strength of the PRF-adhesive is higher than for the PUR (Table 1), but the estimated shear strength from the simulations is not! Clearly, the material parameters chosen in this investigation reflect the above discussion about *several* parameters influencing joint strength, local bond strength *being only one of these*. In the current case, the lesser apparent shear strength of the PRF-adhesive can be explained in terms of effective fracture energy, i.e. the amount of fracture energy that has dissipated at global collapse. From Figure 4 it is clear that a large amount of the PRF-adhesive fracture energy is activated at large shear slips. For the present joint however, the global collapse occurs before these large slips can develop. Consequently, a major part of the PRF-bond line is in a state of deformation belonging to the "left part" of the curve in Figure 4. For the PUR-adhesive the global failure occurs when a major part of its fracture energy has been activated. In Figure 16, this is shown schematically.

Another observation made from the simulations is the extremely large influence of non-parallel end-grain sides of the specimen. For the brittle adhesive, the predicted load bearing capacity of the joint is lowered approximately 20% at a 1° slope (cf. prf01 and prf06). The slope, although small, will result in an eccentric loading of the specimen and severely affect its load-bearing capacity.

[1] The ultimate load for the symmetric *half*.
[2] The values are derived from global load divided by fracture area and include frictional forces.
[3] "True stress values" i.e. the values are derived from the calculated stress distribution in the bond line.

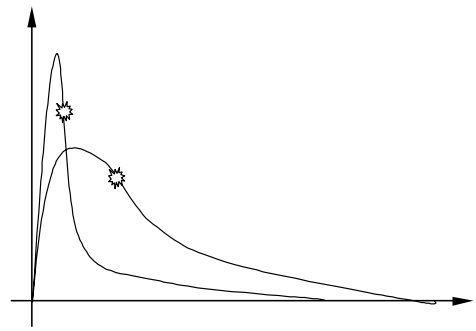

Figure 16. Stress-slip relations with different effective fracture energies. The effective fracture energy means the area beneath the respective curve up to the point of failure.

If the specimen is placed such that the short vertical sides are in contact with the loading device, friction will be included in the forces measured. In order to avoid friction, the test specimen can be placed in a holder, which leaves a gap large enough to ensure that no contact establishes. Another way is, of course, to lubricate, by means of oil, grease or a thin Teflon film. One drawback is that eccentric loading introduces a larger amount of peel stress in the bond line, which will affect the load-bearing capacity of the specimen and thereby the estimated shear strength of the bond line. The response in terms of "measured" average shear stress versus displacement is shown in Figure 17, for the cases "01" and "05", in order to show the influence of the frictional forces. Clearly the friction to the sides can play a decisive role in the evaluation of the test results. As an example, for the PUR-adhesive the average shear stress at maximum load is 11.5 MPa for μ=0.3 ("pur01") and 9.5 MPa for the case of μ=0 ("pur05"). It should also be mentioned that the frictional forces on the horizontal surfaces are beneficial from a load-bearing capacity point of view. This is because the frictional force, if large enough, can prevent tensile peel stresses to develop. For details, see the stress distributions in Appendix A.

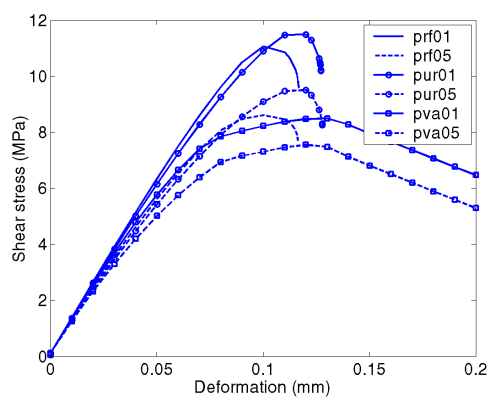

Figure 17. Average shear stress versus displacement for some of the investigated cases.

The overlap length of the specimen is rather large (approx. 38 mm) which leads to a non-uniform stress distribution. This is evident from Figure 18, which shows the stress distribution in the bond line at the edge of the specimen and along its plane of symmetry. For this case there is a negligible "3D-effect", since the material directions of the wood are assumed to coincide with the global coordinate directions.

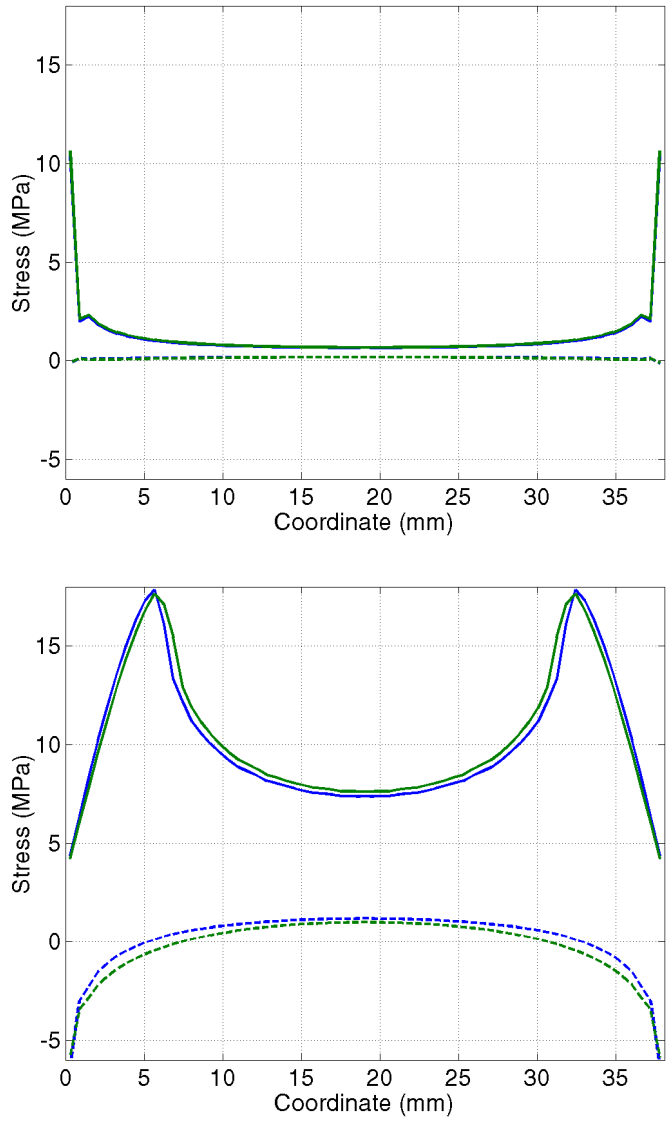

Figure 18. Stress distributions, prf01. Linear elastic state (top) and maximum load (bottom), ASTM-D905. Solid lines are for shear stress and dashed for normal (peel) stress. The different curves are at the edge (green) and in the centre (blue) respectively.

The non-uniform stress distribution leads to a severe underestimation of the local bond strength. The load bearing capacity of the "prf01" specimen is 21.4 kN, which corresponds to an average shear stress of 11.06 MPa. The normalised strength, τ^*, is thus equal to 11.06/18=0.61. In other words, for this extremely brittle adhesive, the D905-specimen underestimates the bond line shear strength by 40%! However, since the measured force in this case includes frictional forces from the contact with the short vertical sides, the situation is even worse: the "true" average shear stress at failure is only 10.0 MPa (i.e. τ^*=0.56).

The stress distributions for the other two adhesives are given in Figure 19 and in Figure 20, respectively. The corresponding normalised shear strengths are τ^*= 0.96 (PUR) and 1.06 (PVAc) including friction, and τ^*= 0.88 and 0.96 for PUR and PVAc respectively as calculated from the stress distribution. In the following average shear stresses are as calculated from the "measured" global load, i.e. including possible frictional forces due to contact with the loading device.

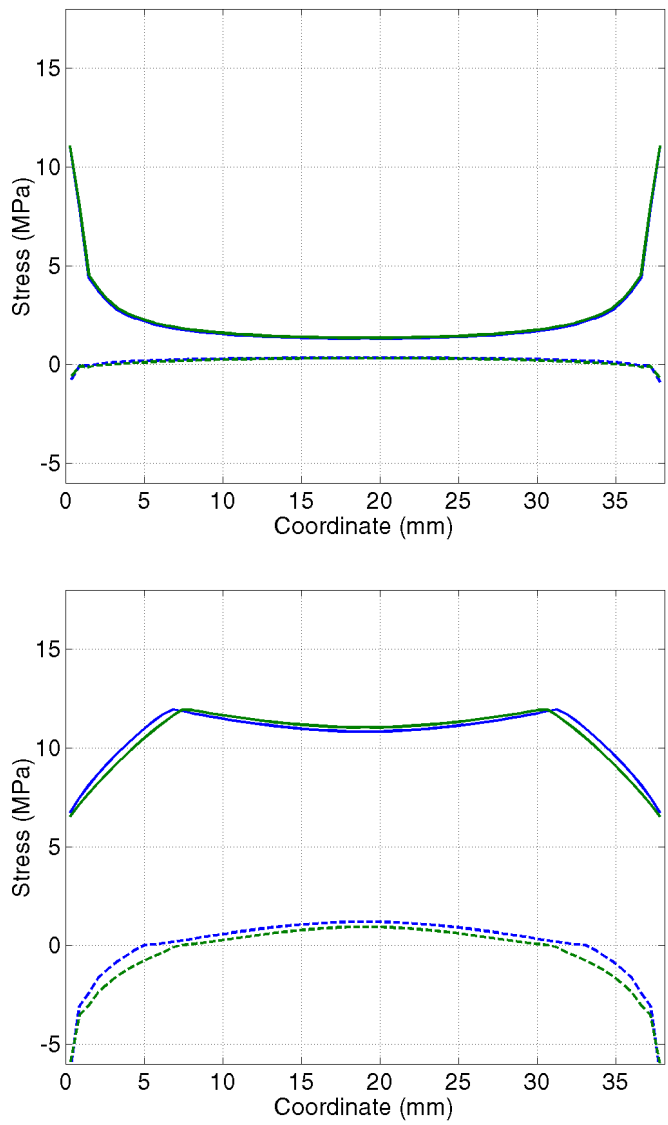

Figure 19. Stress distribution for the case pur01. Linear elastic state (top) and maximum load (bottom), ASTM-D905. Solid lines are for shear stress and dashed for normal (peel) stress. The different curves are at the edge (green) and in the centre (blue) respectively.

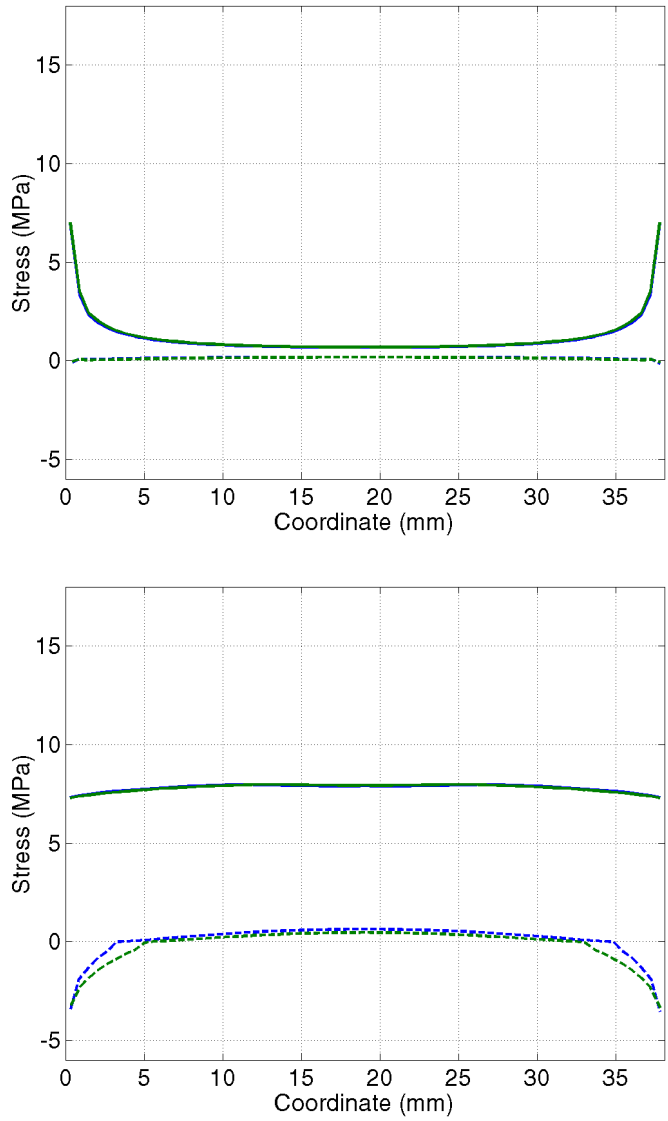

Figure 20. Stress distribution for the case pva01. Linear elastic state (top) and maximum load (bottom), ASTM-D905. Solid lines are for shear stress and dashed for normal (peel) stress. The different curves are at the edge (green) and in the centre (blue) respectively.

The remaining investigated cases are reported in detail in Appendix A.

4.3 ASTM D3535

The deformed state of the specimen for case "prf01" is shown in Figure 21, with deformations scaled by a factor of 10. The results from the simulations are summarised in Table 7, giving load-bearing capacities and corresponding average shear stress at failure.

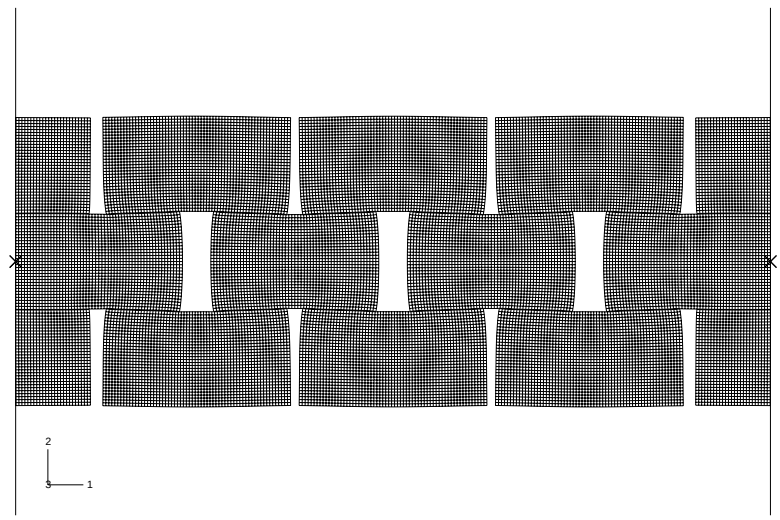

Figure 21. Deformed plot of prf01-specimen.

Table 7. Results from simulations of the ASTM D3535 specimen.

Name	P_{ult} (kN)	τ (MPa)	τ^* (-)
PRF01	19.16	15.33	0.85
PUR01	14.47	11.58	0.96
PVA01	9.93	7.94	0.99
PRF02	18.43	14.75	0.82
PUR02	12.74	10.19	0.85
PVA02	9.77	7.82	0.98
PRF03	16.33	13.06	0.73
PUR03	12.81	10.25	0.85
PVA03	9.14	7.31	0.91
PRF04	14.08	11.26	0.63
PUR04	11.18	8.94	0.75
PVA04	8.09	6.48	0.81
PRF05	16.30	13.04	0.72
PUR05	13.27	10.61	0.88
PVA05	9.40	7.52	0.94
PRF06	13.97	11.17	0.62
PUR06	11.41	9.12	0.76
PVA06	8.85	7.08	0.88

The stress distribution at a linear elastic state and at maximum load for the case "prf01" is shown in Figure 22. The short overlap length (12.5 mm) results in a fairly uniform stress distribution, as compared with the ASTM D905 specimen. This in combination with the compressive stresses perpendicular to the bond line at the ends of each bond line results in a fairly good prediction of local strength.

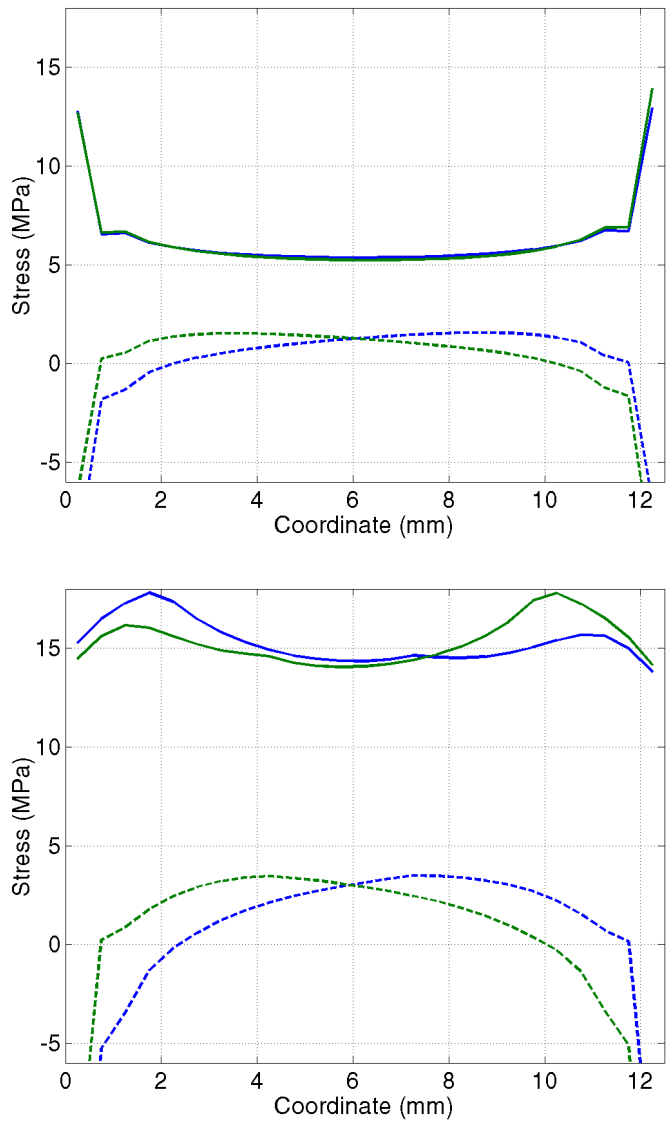

Figure 22. Stress distribution for the case prf01. Linear elastic state (top) and maximum load (bottom), ASTM-D3535. Solid lines are for shear stress and dashed for normal (peel) stress. The different curves are at the first (blue) and second (green) bond lines respectively.

The most important drawback associated with the use of this specimen is related to its size. For each test, a total of 12 bond lines are tested simultaneously and the specimen will fail when the first bond line, i.e. probably the weakest one, fails. This results in an estimate of the strength of the weakest bond line from a group of 12. Such a result cannot be directly compared with results obtained in tests performed with a single bond line at a time. Consider the following example:

> Assume that the stress distribution in the twelve bond lines are equal, and that the normalised strength of each bond line has a coefficient of variation of 20%. Furthermore, the system of bond lines is treated as a weakest link system, and the normalised strength of a bond line is described by a two-parameter Weibull-distribution. For this case the mean load bearing capacity of the specimen will correspond to approximately 65% of the mean capacity of each bond line. This is for the case that all the 12 active bond lines are considered to be a weakest-link system (series system). If, however, the specimen is regarded as being composed of two (independent) series systems, each with 6 bond lines, the corresponding mean load bearing capacity would be approximately 73%.

For Weibull-distributed bond line strengths, the coefficient of variation (COV) of the specimen strength is the same as the COV of its individual bond lines, but for other distributions this is not the case. Therefore any results obtained with this specimen are difficult to compare to results obtained with other single-bond line specimens since both the bond line strength prediction and its variance are affected.

Another way to investigate this effect without using stochastic FE-analyses is to change the strength of only some of the active bond lines in the specimen. This was done for an additional three simulations for the PUR01 case, in which the local strength of one bond line, as indicated in Figure 23, was lowered by 5, 15 and 25% respectively. The resulting load-bearing capacities where found to be 4.3, 13.2 and 22.9% lower than for the case where all the bond lines had the same local strength. Obviously this type of specimen gives a measure of the weakest link in a chain of 12 active bond lines, more than it measures the average local strength.

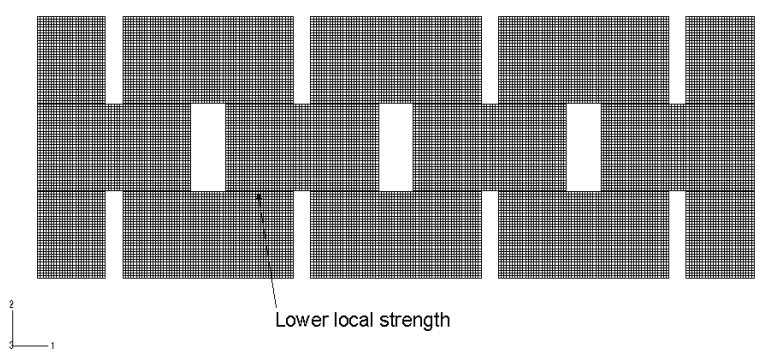

Figure 23. The bond line was assigned 5, 15 and 25% lower local strength values in three additional simulations.

4.4 EN-302-1

The deformed specimen "prf01" is shown in Figure 24 with deformations magnified by a factor of 10, for clarity. From the deformations, it is clear that tensile stresses perpendicular to the bond line develops. These stresses result in a mixed mode state of stress that can affect severely the load bearing capacity of the specimen, and thereby the bond line strength estimate. The results from the simulations are summarised in Table 8, giving load-bearing capacities and corresponding average shear stress at failure.

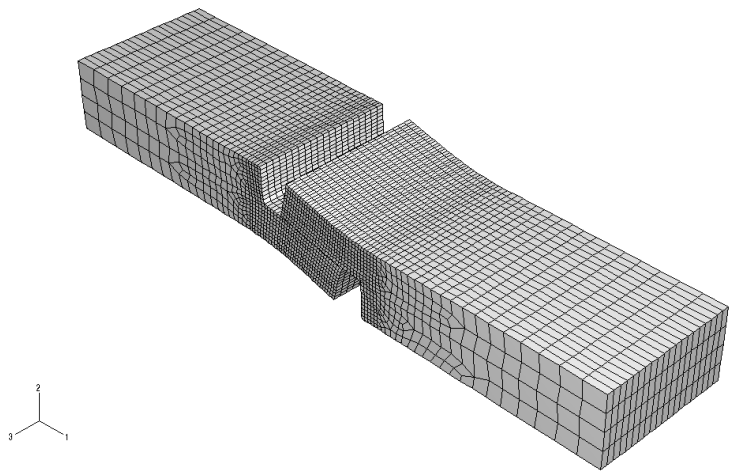

Figure 24. Deformed EN302-1 specimen, prf01.

The severe state of stress in the bond line is shown in Figure 25, with the linear elastic stress distribution and the stress distribution at maximum load for the case "prf01". Clearly the tensile stresses perpendicular to the bond line affects the load bearing capacity of this specimen. However, note that since the strength in tension perpendicular to the bond line is assumed equal for the three adhesives, the "relative" strength (relative to the bond line shear strength) is low for the PRF-adhesive. If the strength perpendicular to the bond line would have been made proportional to the shear strength, the results for the PRF would probably be different, and more like the ones obtained for the PUR and PVA adhesives. The eccentric loading of this specimen also yields rather low strength predictions. This could possibly be avoided by using pinned supports at both ends.

Table 8. Results from simulations of the EN302-1 specimen.

Name	P_{ult} (kN)	τ (MPa)	τ^* (-)
PRF01	2.73	13.66	0.76
PUR01	2.24	11.20	0.93
PVA01	1.57	7.86	0.98
PRF02	2.34	11.68	0.65
PUR02	1.97	9.85	0.82
PVA02	1.40	7.01	0.88
PRF03	2.01	10.04	0.56
PUR03	1.71	8.57	0.71
PVA03	1.26	6.28	0.78
PRF04	1.56	7.81	0.43
PUR04	1.36	6.78	0.57
PVA04	1.04	5.20	0.65
PRF05	1.70	8.49	0.47
PUR05	1.75	8.73	0.73
PVA05	1.33	6.66	0.83
PRF06	1.62	8.11	0.45
PUR06	1.58	7.92	0.66
PVA06	1.22	6.09	0.76
PRF07	1.39	6.94	0.39
PUR07	1.30	6.48	0.54
PVA07	1.01	5.04	0.63
PRF08	1.08	5.42	0.30
PUR08	1.14	5.69	0.47
PVA08	0.93	4.67	0.58

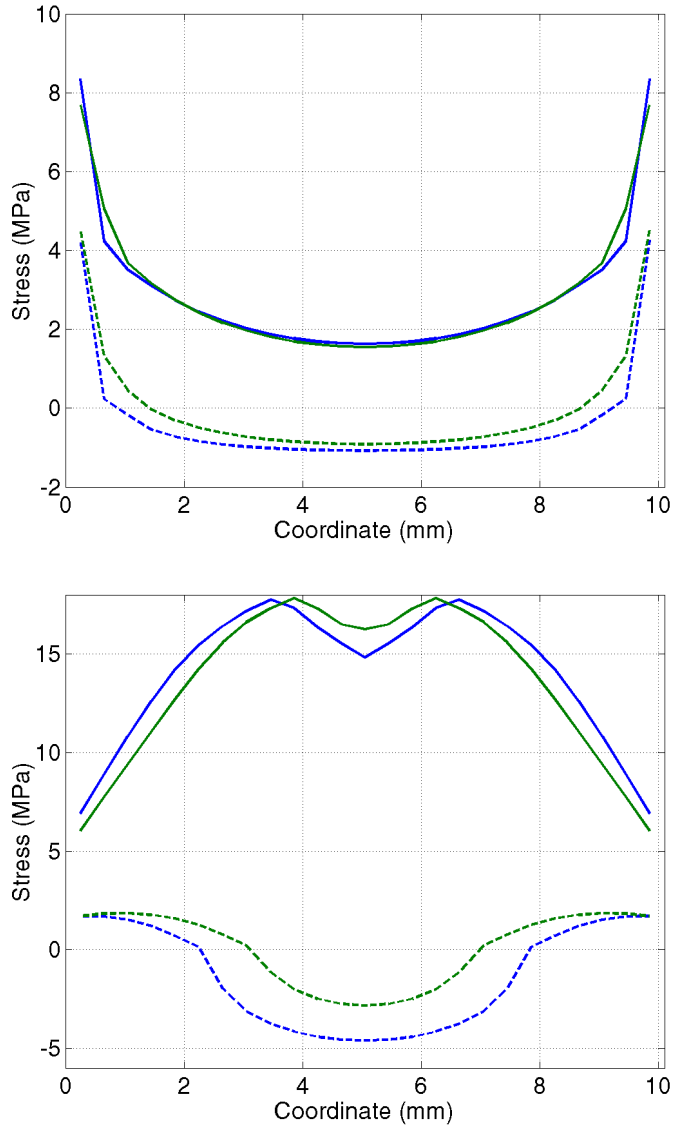

Figure 25. Stress distribution for the case prf01. Linear elastic state (top) and maximum load (bottom), EN302-1. Solid lines are for shear stress and dashed for normal (peel) stress. The different curves are at the edge (blue) and in the centre (green) of the specimen respectively.

4.5 ASTM D4680

The deformed specimen at maximum load for the cases “prf01” is shown in Figure 26. The deformations are scaled by a factor of 10, for clarity. For this case there is contact between the short vertical sides of the specimen and the loading surfaces.

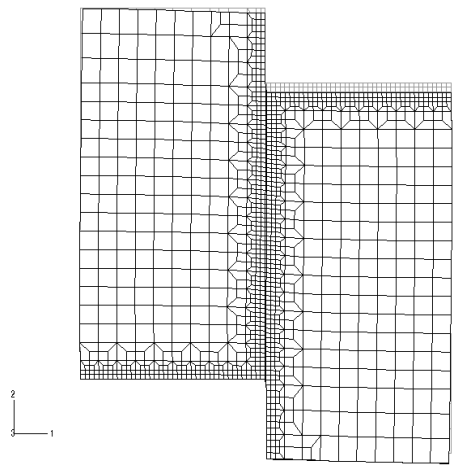

Figure 26. Deformed plot of prf01-specimen. Undeformed plot is superimposed.

The results from the simulations are summarised in Table 9, giving load-bearing capacities and corresponding average shear stress at failure, calculated by dividing the maximum load by the nominal fracture area. Also the average shear stress calculated from the shear stress distribution along the bond line is given. This in an attempt to disregard any influence of frictional forces. Since this specimen is similar to the D905 specimen, the general conclusions drawn for that specimen are also valid here. Consequently it is difficult to rank the two stronger adhesives in the “correct” order in terms of local strength, see e.g. “PRF01” and “PRF03” as compared to “PUR01” and “PUR03”. These cases show that an eccentric loading is more severe for the most brittle adhesive, and so severe that it can affect the prediction of local strength severely.

Table 9. Results from simulations of the D4680 specimen.

Name	P_{ult} (kN)[1]	τ (MPa)[2]	τ* (-)[2]	τ (MPa)[3]	τ* (-)[3]
PRF01	4.18	12.9	0.72	11.9	0.66
PUR01	3.94	12.2	1.02	11.2	0.93
PVA01	2.77	8.60	1.07	7.87	0.98
PRF02	3.87	12.0	0.67	11.5	0.64
PUR02	3.76	11.7	0.97	11.2	0.93
PVA02	2.66	8.24	1.03	7.89	0.99
PRF03	3.54	11.0	0.61	10.5	0.58
PUR03	3.68	11.4	0.95	10.9	0.91
PVA03	2.65	8.23	1.03	7.84	0.98
PRF04	3.08	9.56	0.53	9.02	0.50
PUR04	3.36	10.4	0.87	9.82	0.82
PVA04	2.65	8.21	1.03	7.74	0.97
PRF05	3.24	10.1	0.56	10.1	0.56
PUR05	3.29	10.2	0.85	10.2	0.85
PVA05	2.44	7.57	0.95	7.57	0.95
PRF06	2.74	8.49	0.47	6.66	0.37
PUR06	2.81	8.71	0.73	6.83	0.57
PVA06	2.42	7.50	0.94	5.84	0.73
PRF07	2.58	8.00	0.44	6.25	0.35
PUR07	2.63	8.17	0.68	6.36	0.53
PVA07	2.37	7.35	0.92	5.71	0.71

The stress distribution at a linear elastic state and at maximum load for the case "prf01" is shown in Figure 27. The shorter overlap length as compared to the D905 specimen results in slightly more uniform stress distribution. However, the general impression is that the prediction of local strength is still not satisfactory.

[1] The ultimate load for the symmetric *half*.
[2] The values are derived from global load divided by fracture area and include frictional forces
[3] "True stress values" i.e. the values are derived from the calculated stress distribution in the bond line.

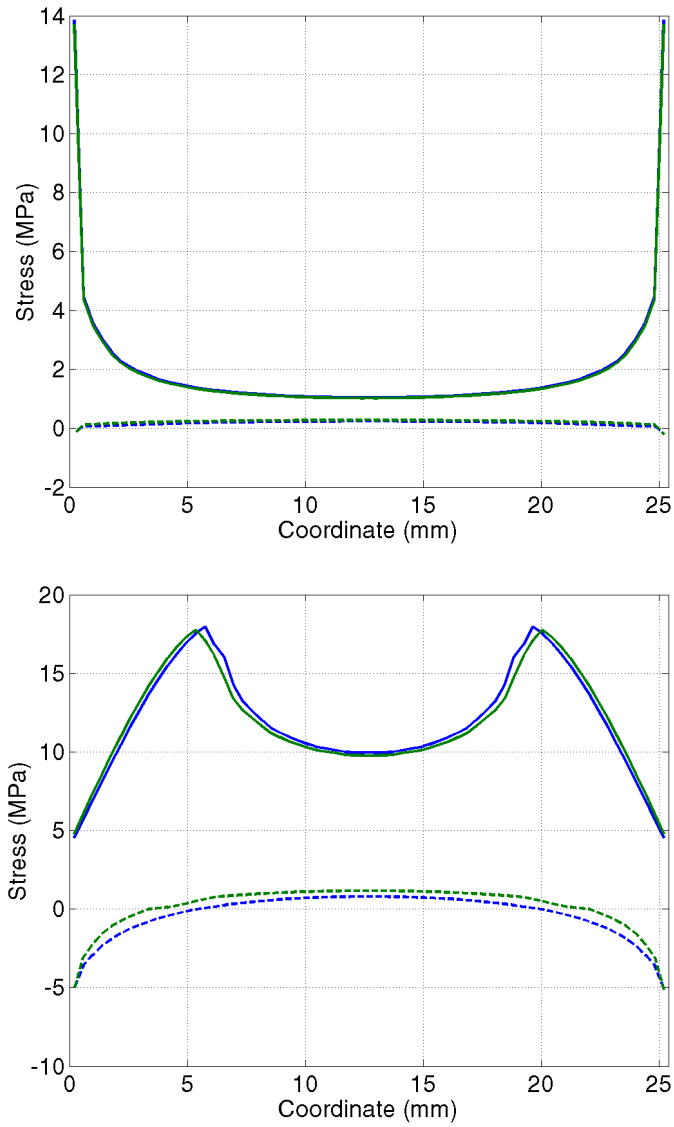

Figure 27. Stress distribution for the case prf01. Linear elastic state (top) and maximum load (bottom), ASTM D4680. Solid lines are for shear stress and dashed for normal (peel) stress. The different curves are at the edge (blue) and in the centre (green) of the specimen respectively.

5 Concluding Remarks

5.1 Conclusions

The following conclusions can be drawn from this study:

- Several parameters influence the load bearing capacity of an adhesive joint:
  - Local bond strength and fracture energy
  - Adherend stiffness
  - Joint size and shape
- For simple evaluation of the local strength of a bond line it is important to obtain a uniform stress distribution in the joint at failure.
- The stress distribution in a joint tends to be more uniform as the size of the joint decreases.
- In order to obtain local strength statistics (e.g. mean values and COV), it is preferable to use several specimens, each with a single bond line, instead of using a complex multi-bond line specimen.
- The ASTM D905 specimen:
  - is fairly large and, as a result gives a non-uniform stress distribution
  - is sensitive to the influence of friction
  - was not able to rank the three adhesives in the correct order in terms of local strength
- The ASTM D3535 specimen:
  - has an extremely complex geometry
  - gives the best estimate of local strength for ideal cases with uniform within-specimen strength, but
  - does not give the local bond strength statistics of a number of individual bond lines, but the statistics of the weakest bond lines in a number of groups, each containing 12 bond lines
- The EN302-1 specimen:
  - has an appealingly short overlap length
  - somewhat surprising, gives results strongly influenced by the bond line mixed-mode behaviour, since there is a considerable amount of positive tensile stresses perpendicular to the bond line. This influence may partly be due to the bond line model parameters employed, since these assumed that the perpendicular-to-grain behaviour was uncorrelated to the behaviour in shearing. Since the *relative* normal strength (relative the shear strength) is much lower for the PRF-adhesive, the specimen gives a rather poor local strength estimate.
  - is sensitive to eccentric loading, at least for the investigated case with fixed support at the one end of the specimen.
- The ASTM D4680 specimen
  - is smaller than the D905 specimen, but has still a large overlap length, resulting in non-uniform stress distributions and poor prediction of local strength
  - is just barely capable of ranking the adhesives in correct order in terms of local strength
  - is also sensitive to the influence of friction.
- *If* measuring local shear strength is the main purpose of the testing the EN302-specimen is recommended, its main advantages being a good compromise

between uniform stress distribution and easy-to-use and manufacture. However, it should preferably be used with both supports pinned, so that no moments are introduced.

5.2 Future Work

Further investigations of the behaviour of the wood adhesive specimens could include experimental studies, in order to verify the simulations. These experiments should then include basic characterisation of the fracture mechanical properties of the bond lines through stable shear and tensile tests. But also tests using the test set-ups investigated here, preferably with deliberately added imperfections such as for example eccentric loading.

Additional FE-simulations could also be of interest, such as investigating:

- The influence of slope of grain
- Influence of the approximately cylindrical orientation of the wood material principal directions
- Other test set-ups, such as using pinned connections for the EN302-1 specimen
- Additional bond line material parameters
- Variation of within-specimen local strength of the bond lines(s)

6 References

Kollmann, F. F. P. and Côté, W. A. (1968). *Principles of Wood Science and Technology*. Springer Verlag, Berlin, Germany.

Serrano, E. (2000). *Adhesive Joints in Timber Engineering. Modelling and testing of fracture properties*. PhD-thesis. Report TVSM-1012. Div. of Structural Mechanics, Lund University, Lund, Sweden.

Wernersson, H. (1994). *Fracture Characterization of Wood Adhesive Joints*. PhD-thesis. Report TVSM-1006. Div. of Structural Mechanics, Lund University, Lund, Sweden.

APPENDIX A: Detailed Results – ASTM D905

Simulation Scheme and Results – ASTM D905

Simulation type, no.	Eccentricity, e (mm)	Coefficient of friction	Slope of end-face
01	0	0.3	0
02	0.5	0.3	0
03	2	0.3	0
04	4	0.3	0
05	0	0	0
06	0	0.3	1°
07	0	0.3	5°

Name	P_{ult} (kN)[1]	τ (MPa)[2]	τ* (-)[2]	τ (MPa)[3]	τ* (-)[3]
PRF01	10.7	11.1	0.61	10.2	0.57
PUR01	11.1	11.5	0.96	10.6	0.88
PVA01	8.22	8.49	1.06	7.80	0.98
PRF02	10.2	10.6	0.58	10.2	0.57
PUR02	10.9	11.3	0.94	10.8	0.90
PVA02	7.90	8.16	1.02	7.8	0.98
PRF03	9.43	9.74	0.54	9.33	0.52
PUR03	10.5	10.8	0.90	10.4	0.86
PVA03	7.93	8.20	1.02	7.82	0.98
PRF04	8.59	8.88	0.49	8.46	0.47
PUR04	9.65	9.98	0.83	9.50	0.79
PVA04	7.86	8.12	1.02	7.71	0.96
PRF05	8.33	8.61	0.48	8.61	0.48
PUR05	9.20	9.51	0.79	9.41	0.78
PVA05	7.30	7.55	0.94	7.47	0.93
PRF06	8.32	8.59	0.48	7.20	0.40
PUR06	9.18	9.49	0.79	7.96	0.66
PVA06	7.70	7.96	0.99	6.59	0.82
PRF07	8.07	8.34	0.46	6.92	0.38
PUR07	8.48	8.76	0.49	7.28	0.40
PVA07	7.44	7.68	0.96	6.35	0.79

[1] The ultimate load for the symmetric *half*.
[2] The values are derived from global load divided by fracture area and include frictional forces
[3] "True stress values" i.e. the values are derived from the calculated stress distribution in the bond line.

Average shear stress versus deformation – ASTM D905

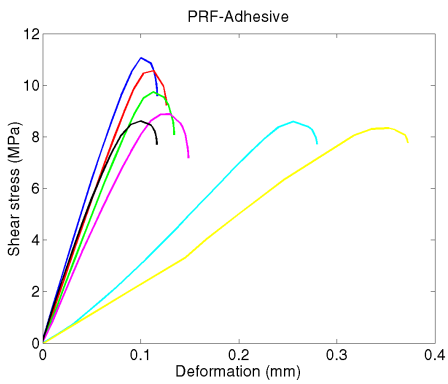

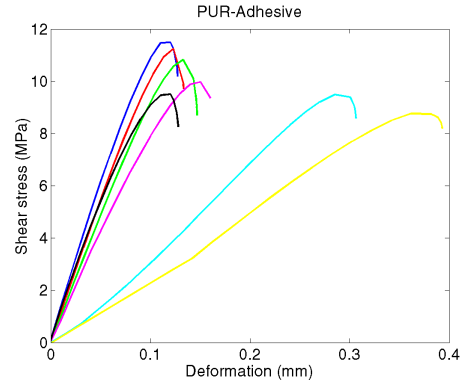

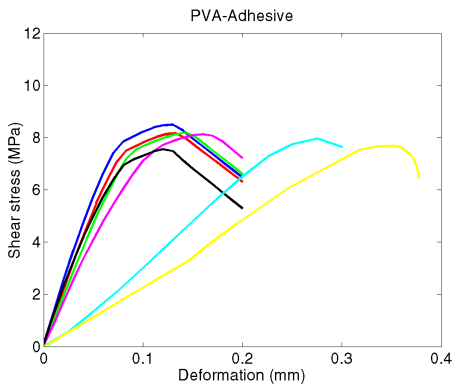

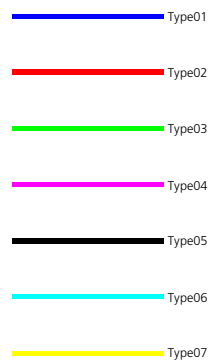

Stress distributions – ASTM D905 – Type 01

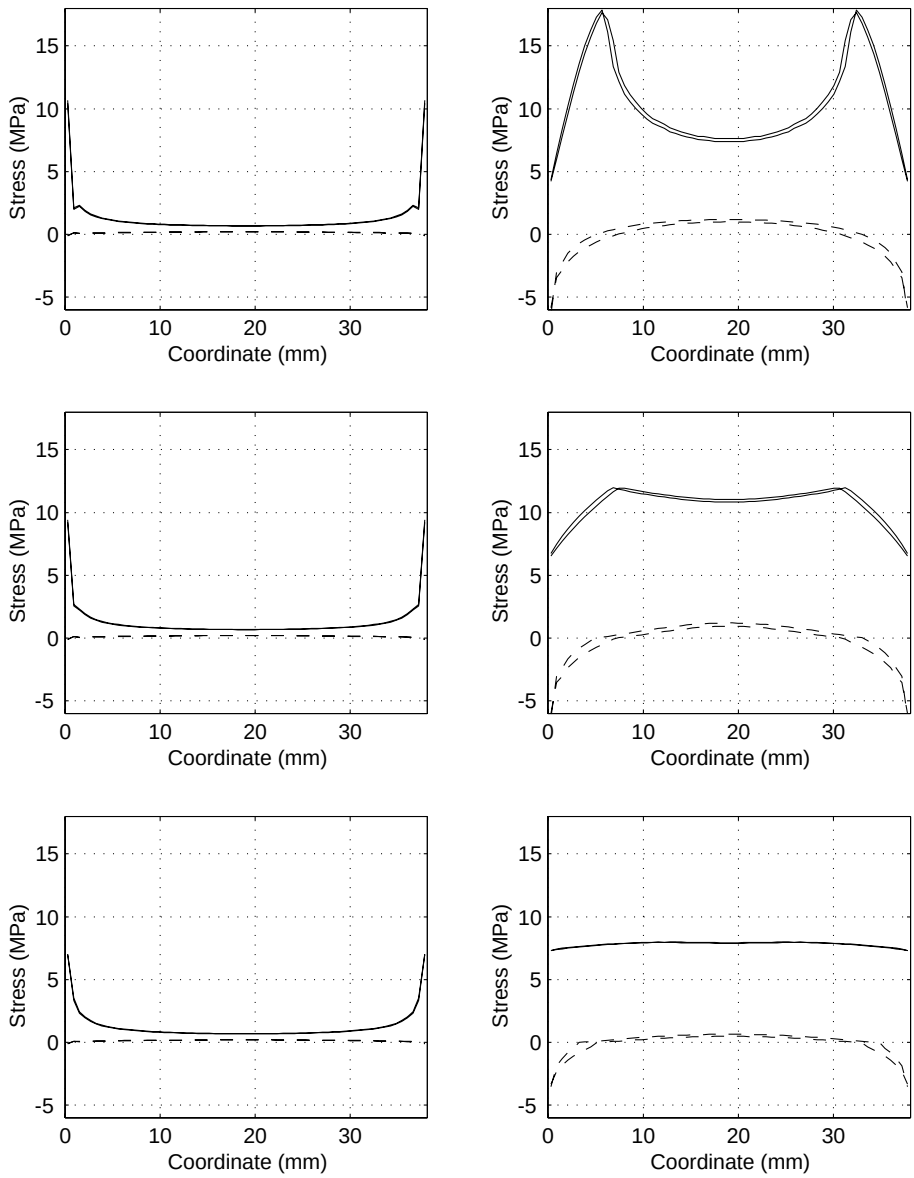

Figure 28. Linear elastic stress distributions (left) and stresses at maximum load (right). PRF (top) PUR (middle) and PVA (bottom). Solid lines are for shear stress and dashed for normal (peel) stress. The different curves are at the edge and in the centre respectively.

Stress distributions – ASTM D905 – Type 02

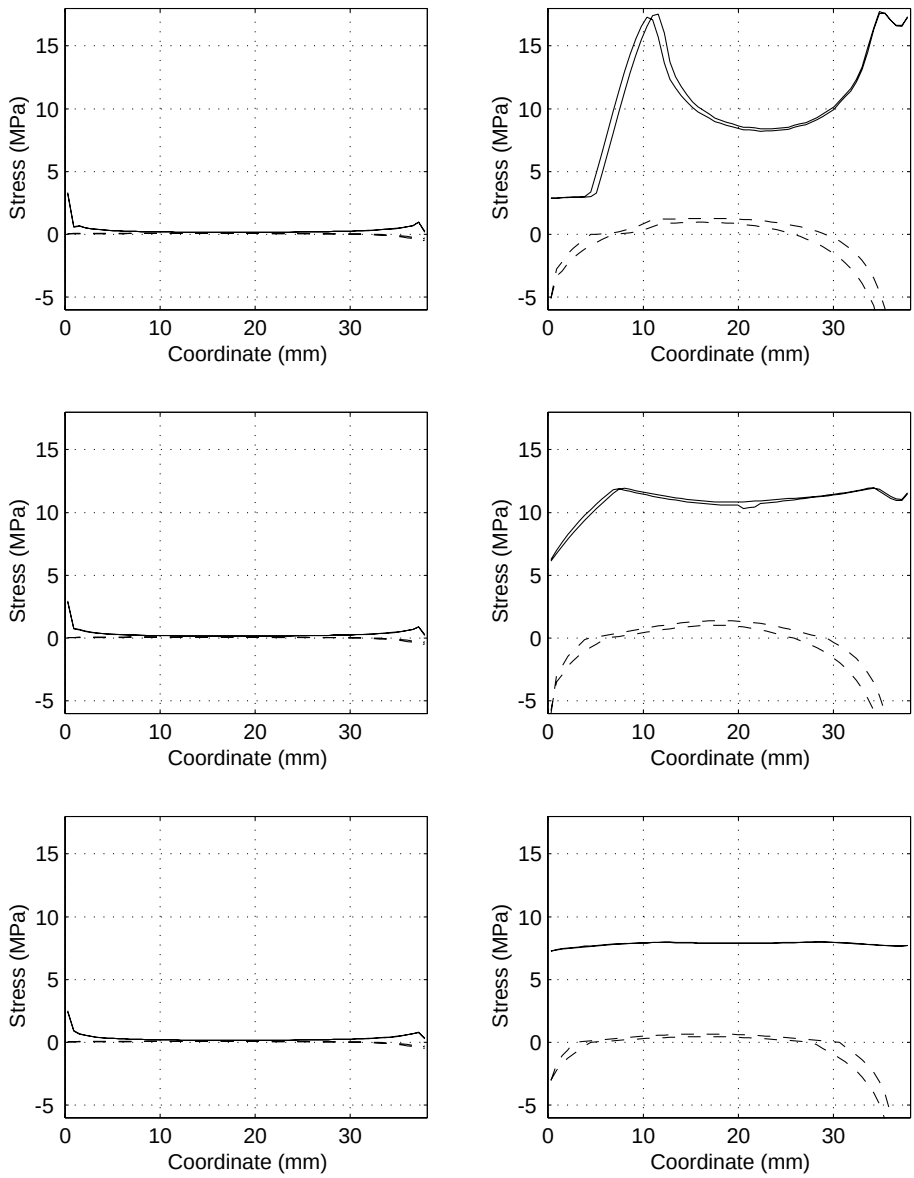

Figure 29 Linear elastic stress distributions (left) and stresses at maximum load (right). PRF (top) PUR (middle) and PVA (bottom). Solid lines are for shear stress and dashed for normal (peel) stress. The different curves are at the edge and in the centre respectively.

Stress distributions – ASTM D905 – Type 03

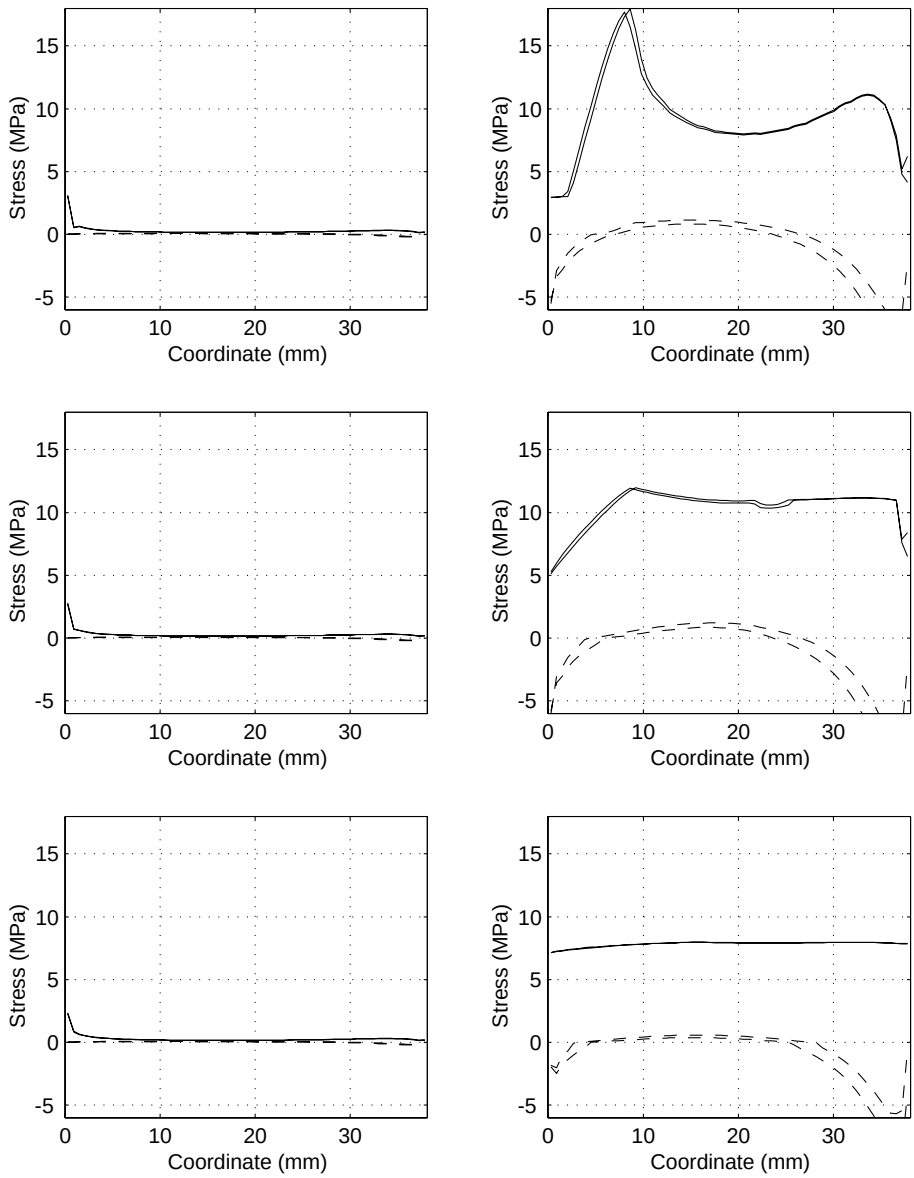

Figure 30 Linear elastic stress distributions (left) and stresses at maximum load (right). PRF (top) PUR (middle) and PVA (bottom). Solid lines are for shear stress and dashed for normal (peel) stress. The different curves are at the edge and in the centre respectively.

Stress distributions – ASTM D905 – Type 04

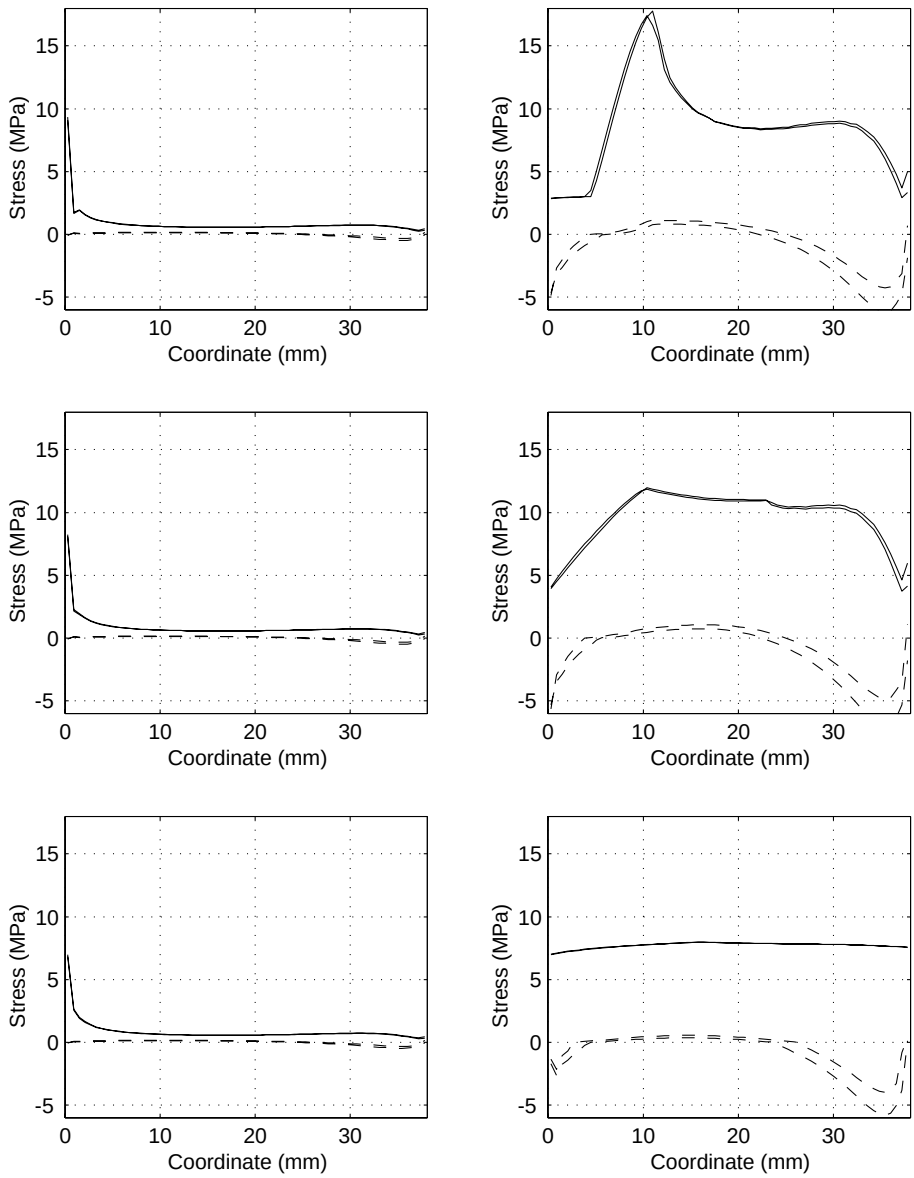

Figure 31 Linear elastic stress distributions (left) and stresses at maximum load (right). PRF (top) PUR (middle) and PVA (bottom). Solid lines are for shear stress and dashed for normal (peel) stress. The different curves are at the edge and in the centre respectively.

Stress distributions – ASTM D905 – Type 05

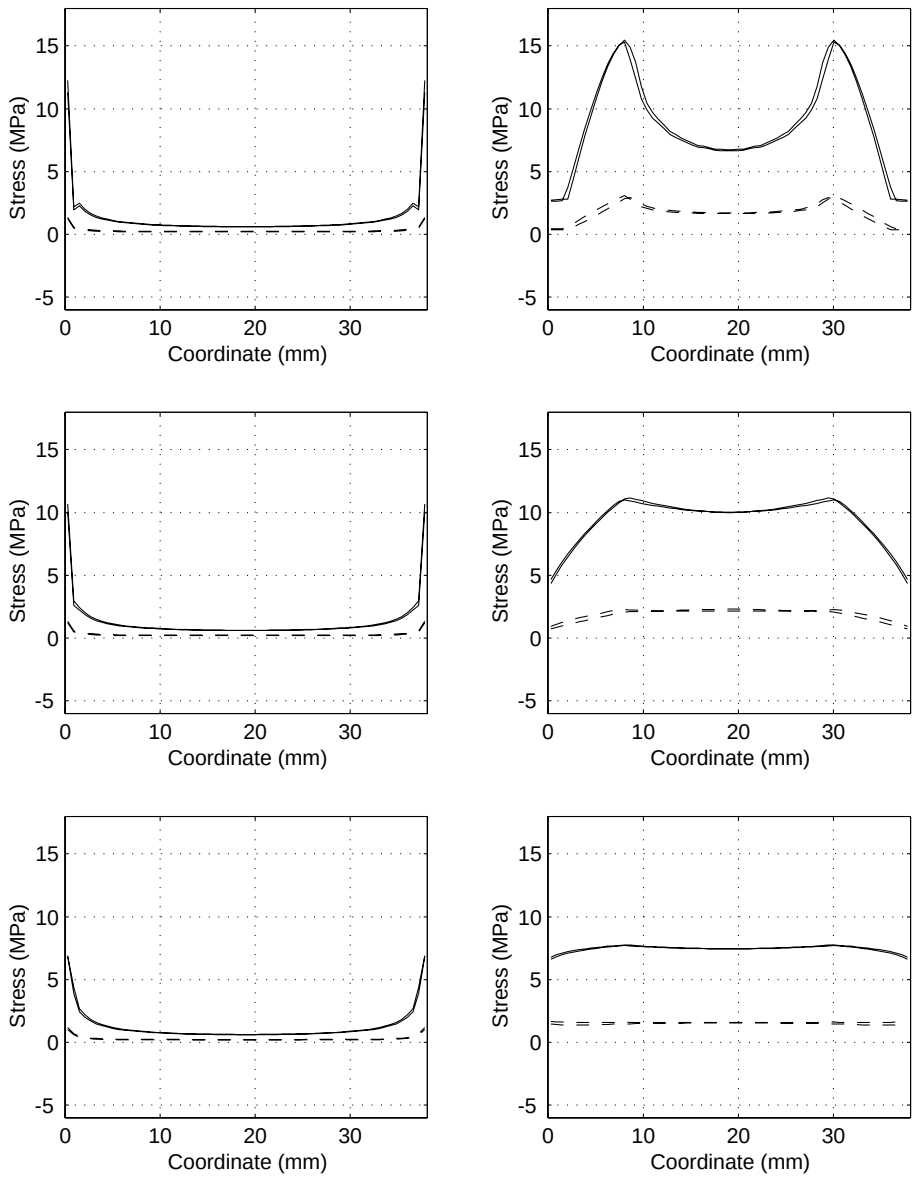

Figure 32 Linear elastic stress distributions (left) and stresses at maximum load (right). PRF (top) PUR (middle) and PVA (bottom). Solid lines are for shear stress and dashed for normal (peel) stress. The different curves are at the edge and in the centre respectively.

Stress distributions – ASTM D905 – Type 06

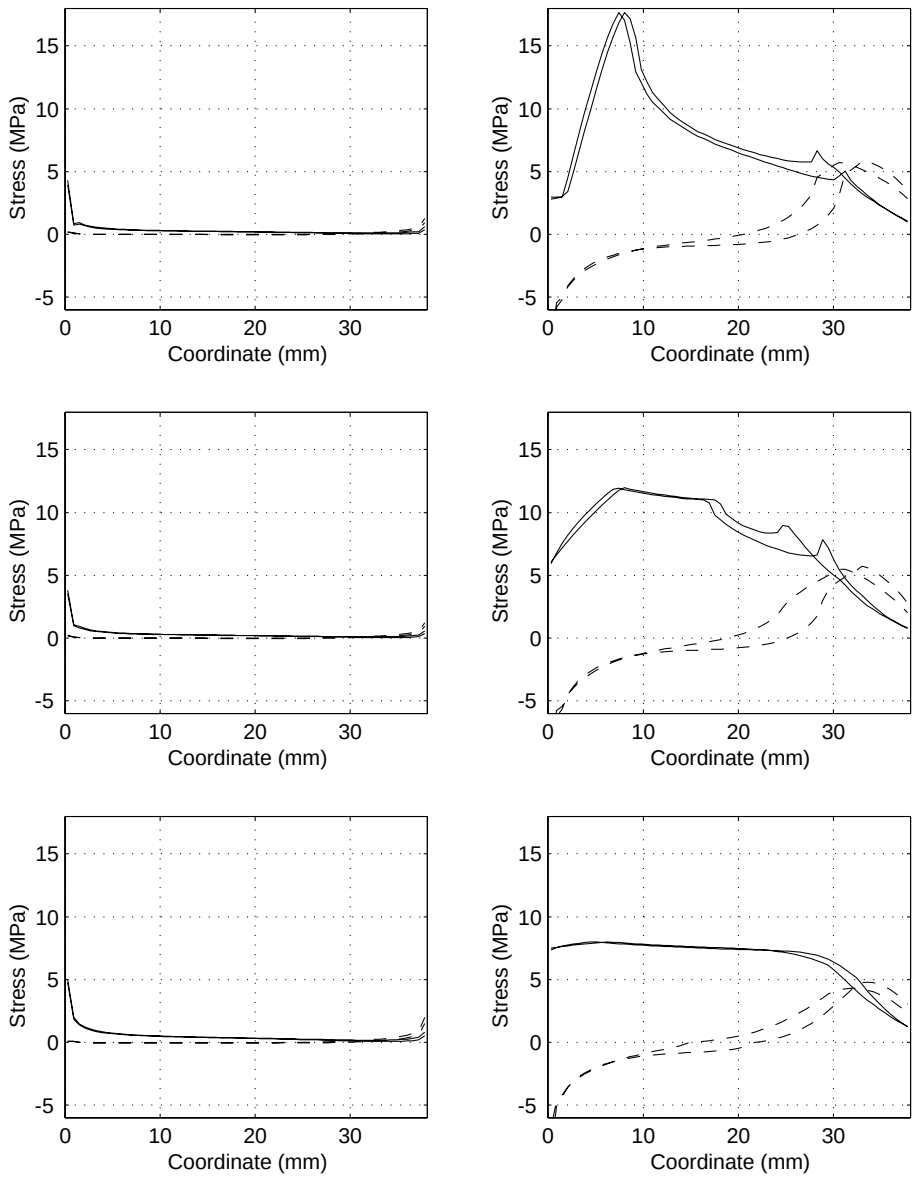

Figure 33 Linear elastic stress distributions (left) and stresses at maximum load (right). PRF (top) PUR (middle) and PVA (bottom). Solid lines are for shear stress and dashed for normal (peel) stress. The different curves are at the edge and in the centre respectively.

Stress distributions – ASTM D905 – Type 07

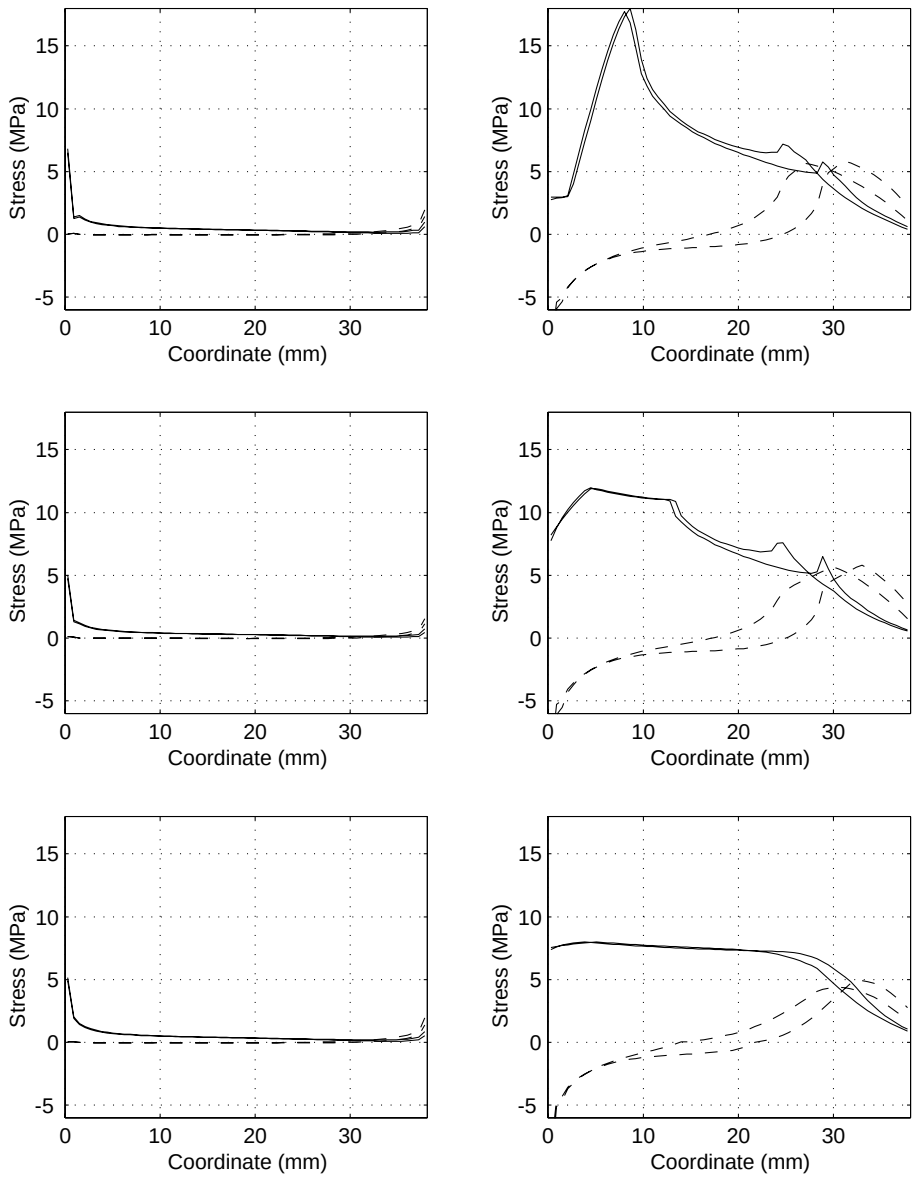

Figure 34 Linear elastic stress distributions (left) and stresses at maximum load (right). PRF (top) PUR (middle) and PVA (bottom). Solid lines are for shear stress and dashed for normal (peel) stress. The different curves are at the edge and in the centre respectively.

APPENDIX B: Detailed Results – ASTM D3535

Simulation Scheme and Results - ASTM D3535

Simulation type no.	eccentricity (mm)	coefficient of friction	prescribed rotation (rad/mm)
01	0	0.3	0
02	0.5	0.3	0
03	2	0.3	0
04	4	0.3	0
05	0	0.3	0.01
06	0	0.3	0.02

Name	P_{ult} (kN)	τ (MPa)	τ^* (-)
PRF01	19.16	15.33	0.85
PUR01	14.47	11.58	0.96
PVA01	9.93	7.94	0.99
PRF02	18.43	14.75	0.82
PUR02	12.74	10.19	0.85
PVA02	9.77	7.82	0.98
PRF03	16.33	13.06	0.73
PUR03	12.81	10.25	0.85
PVA03	9.14	7.31	0.91
PRF04	14.08	11.26	0.63
PUR04	11.18	8.94	0.75
PVA04	8.09	6.48	0.81
PRF05	16.30	13.04	0.72
PUR05	13.27	10.61	0.88
PVA05	9.40	7.52	0.94
PRF06	13.97	11.17	0.62
PUR06	11.41	9.12	0.76
PVA06	8.85	7.08	0.88

Average shear stress versus deformation – ASTM D3535

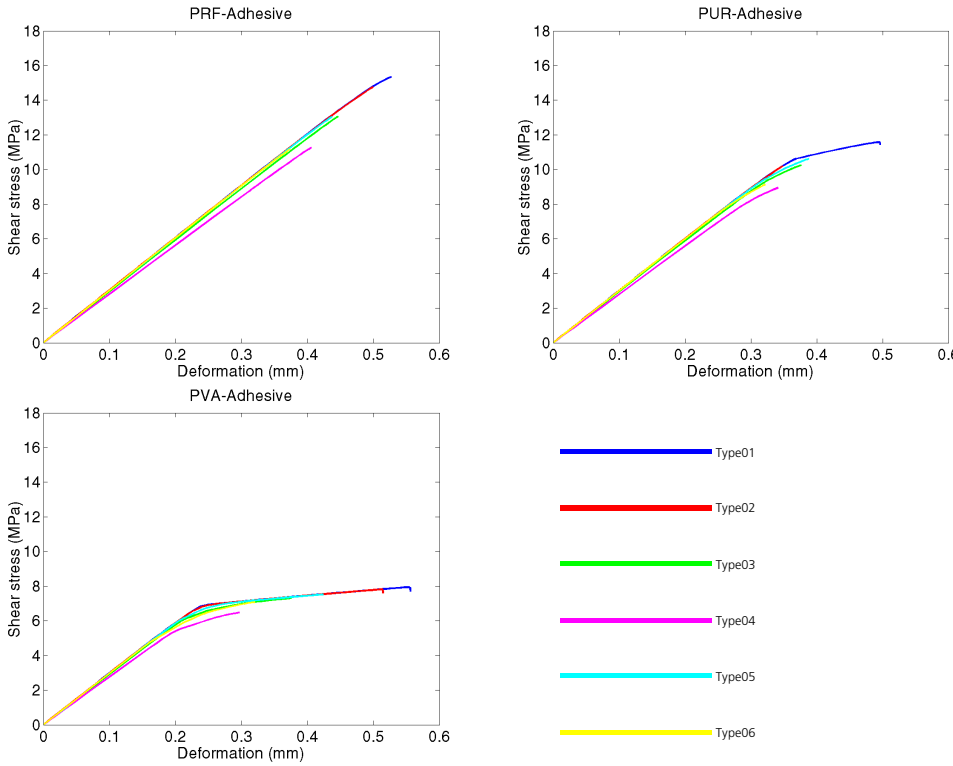

Stress distributions – ASTM D3535 – Type 01

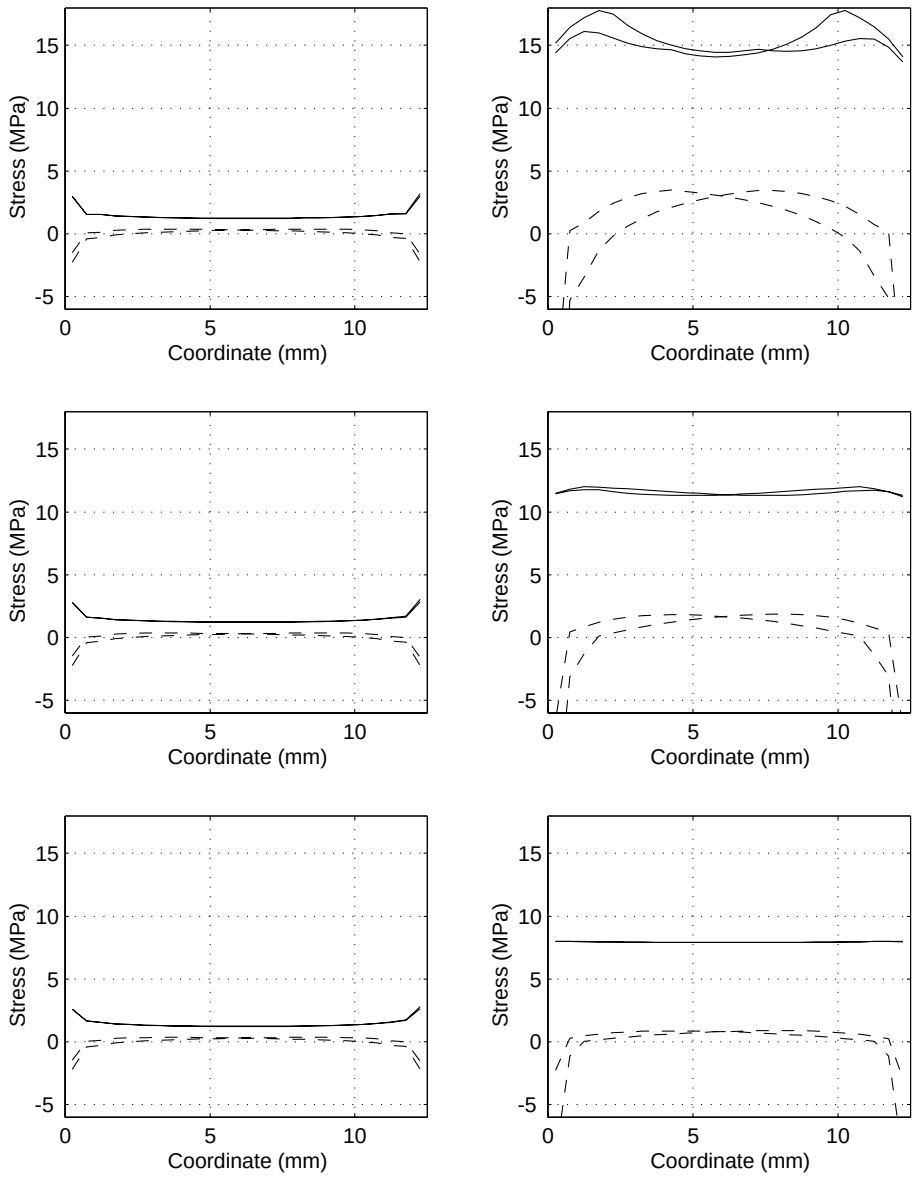

Figure 35 Linear elastic stress distributions (left) and stresses at maximum load (right). PRF (top) PUR (middle) and PVA (bottom). Solid lines are for shear stress and dashed for normal (peel) stress. The different curves are at the first and second bond line respectively.

Stress distributions – ASTM D3535 – Type 02

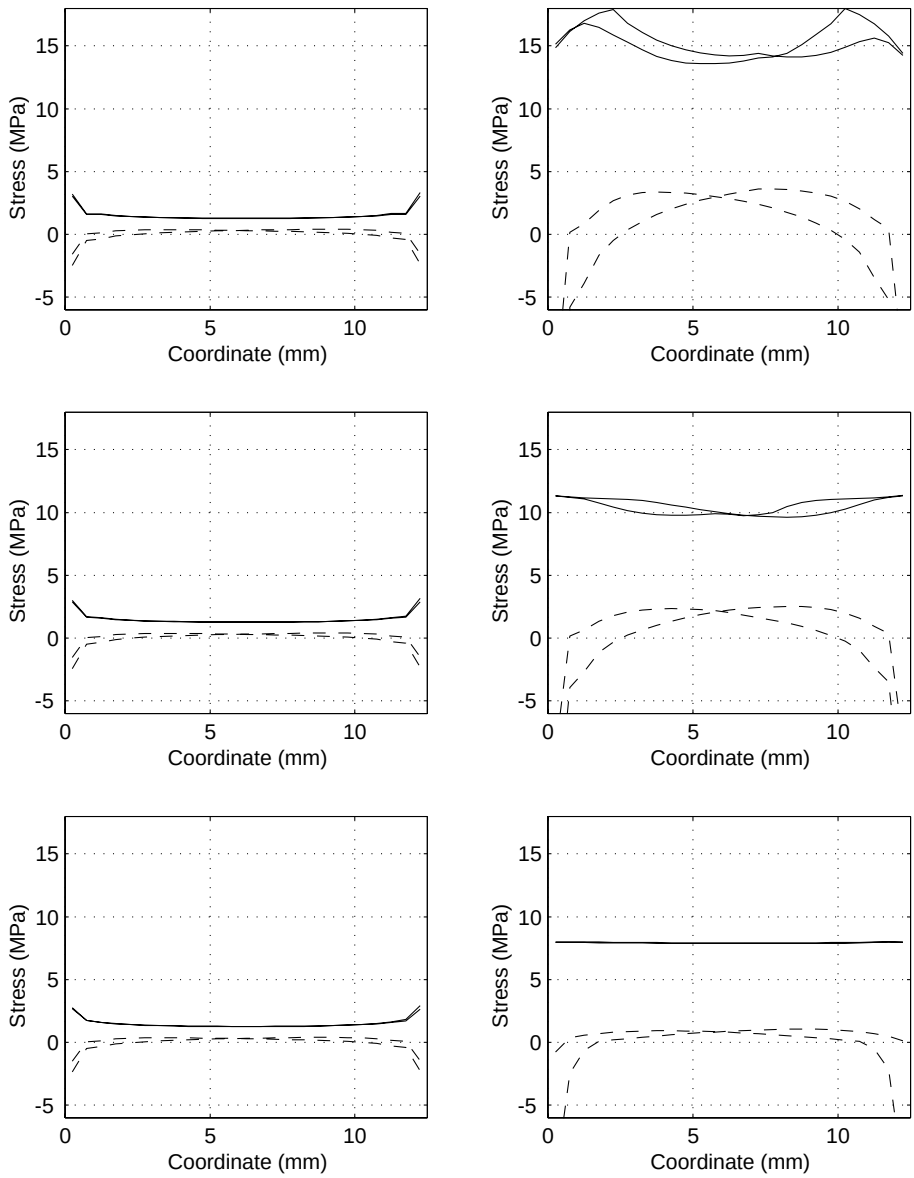

Figure 36 Linear elastic stress distributions (left) and stresses at maximum load (right). PRF (top) PUR (middle) and PVA (bottom). Solid lines are for shear stress and dashed for normal (peel) stress. The different curves are at the first and second bond line respectively.

Stress distributions – ASTM D3535 – Type 03

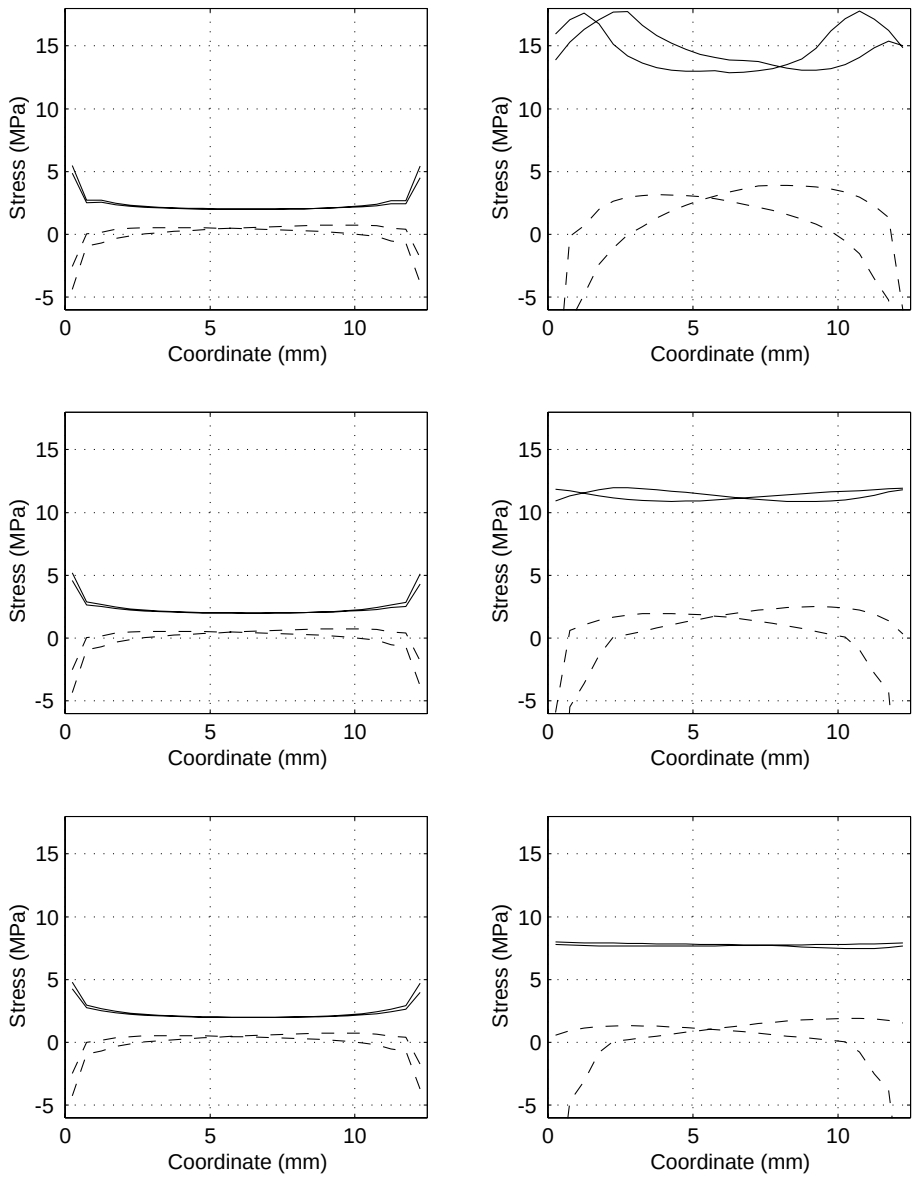

Figure 37 Linear elastic stress distributions (left) and stresses at maximum load (right). PRF (top) PUR (middle) and PVA (bottom). Solid lines are for shear stress and dashed for normal (peel) stress. The different curves are at the first and second bond line respectively.

Stress distributions – ASTM D3535 – Type 04

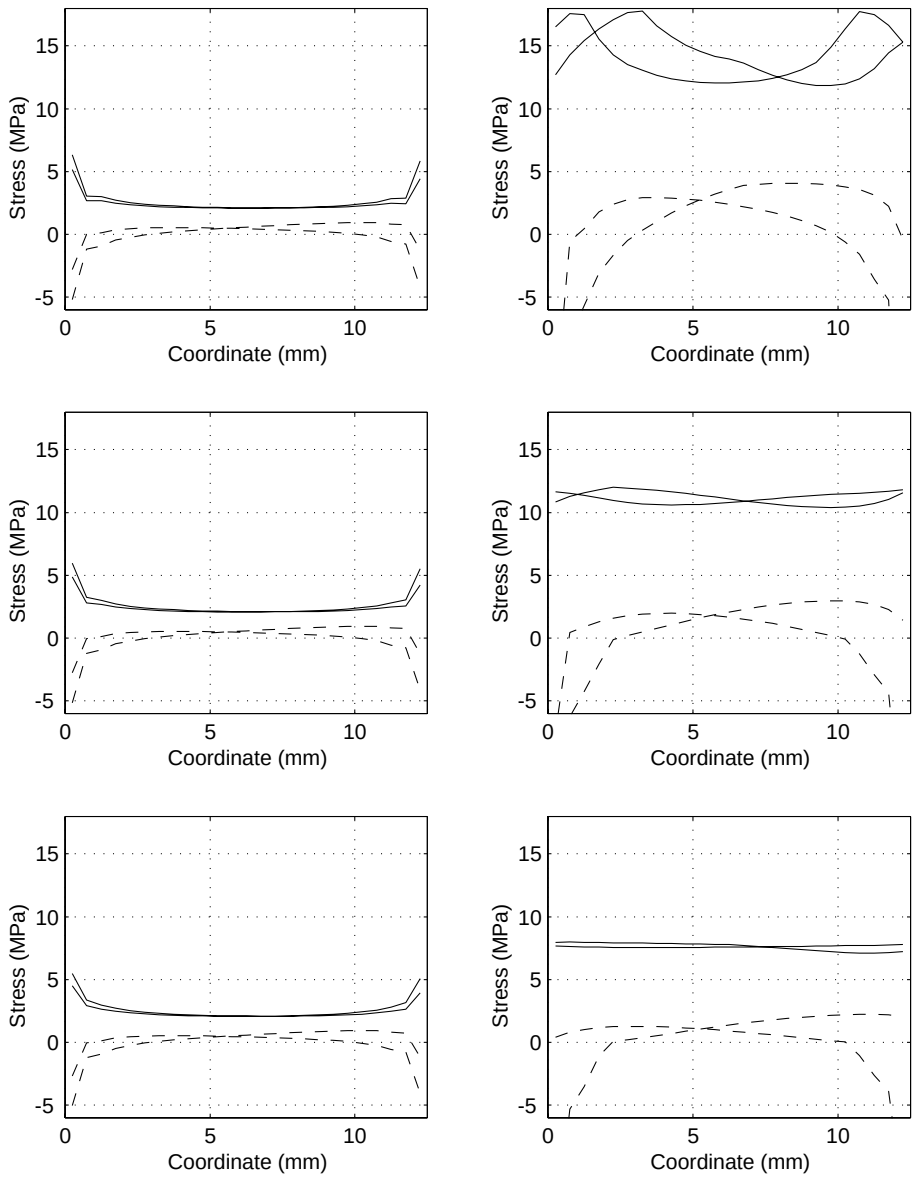

Figure 38 Linear elastic stress distributions (left) and stresses at maximum load (right). PRF (top) PUR (middle) and PVA (bottom). Solid lines are for shear stress and dashed for normal (peel) stress. The different curves are at the first and second bond line respectively.

Stress distributions – ASTM D3535 – Type 05

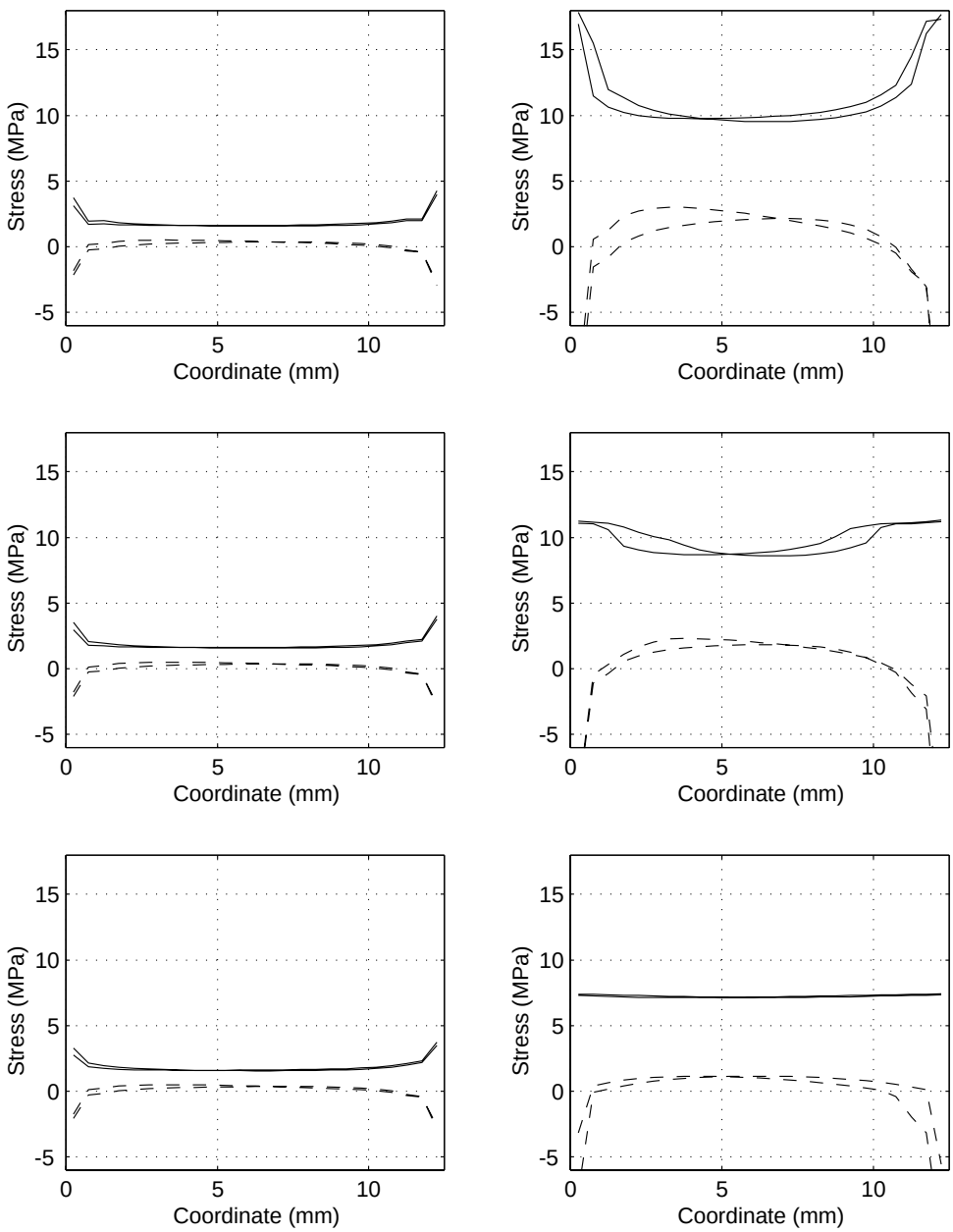

Figure 39 Linear elastic stress distributions (left) and stresses at maximum load (right). PRF (top) PUR (middle) and PVA (bottom). Solid lines are for shear stress and dashed for normal (peel) stress. The different curves are at the first and second bond line respectively.

Stress distributions – ASTM D3535 – Type 06

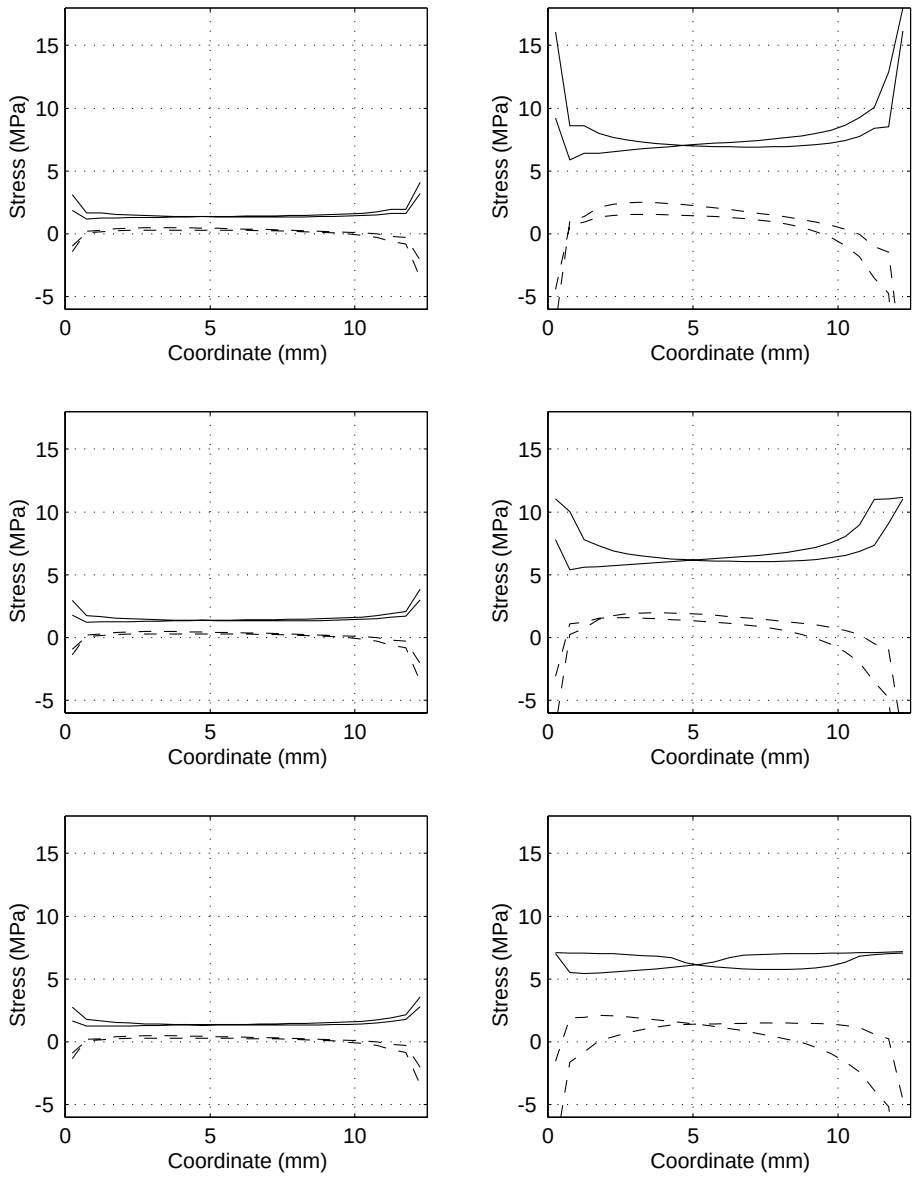

Figure 40 Linear elastic stress distributions (left) and stresses at maximum load (right). PRF (top) PUR (middle) and PVA (bottom). Solid lines are for shear stress and dashed for normal (peel) stress. The different curves are at the first and second bond line respectively.

APPENDIX C: Detailed Results – EN302-1

Simulation Scheme and Results – EN302-1

Simulation type no.	eccentricity, e_z (mm)	eccentricity, e_y (mm)
01	0	0
02	1	0
03	2	0
04	4	0
05	1	1
06	2	1
07	4	1
08	4	2

Name	P_{ult} (kN)	τ (MPa)	τ^* (-)
PRF01	2.73	13.66	0.76
PUR01	2.24	11.20	0.93
PVA01	1.57	7.86	0.98
PRF02	2.34	11.68	0.65
PUR02	1.97	9.85	0.82
PVA02	1.40	7.01	0.88
PRF03	2.01	10.04	0.56
PUR03	1.71	8.57	0.71
PVA03	1.26	6.28	0.78
PRF04	1.56	7.81	0.43
PUR04	1.36	6.78	0.57
PVA04	1.04	5.20	0.65
PRF05	1.70	8.49	0.47
PUR05	1.75	8.73	0.73
PVA05	1.33	6.66	0.83
PRF06	1.62	8.11	0.45
PUR06	1.58	7.92	0.66
PVA06	1.22	6.09	0.76
PRF07	1.39	6.94	0.39
PUR07	1.30	6.48	0.54
PVA07	1.01	5.04	0.63
PRF08	1.08	5.42	0.30
PUR08	1.14	5.69	0.47
PVA08	0.93	4.67	0.58

Average shear stress versus deformation – EN302-1

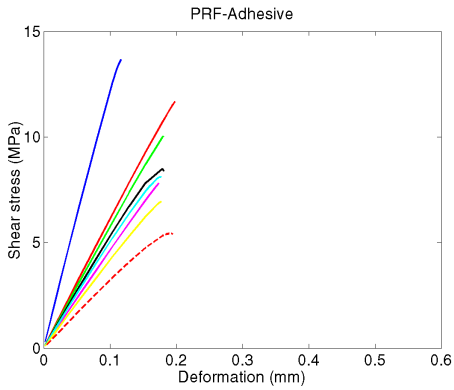

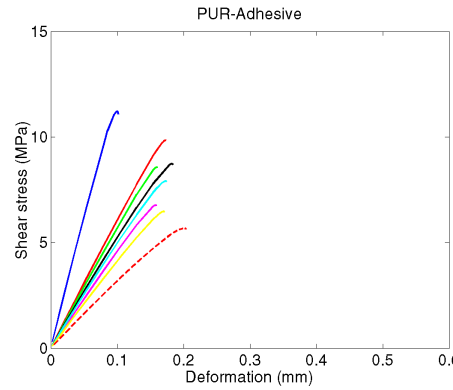

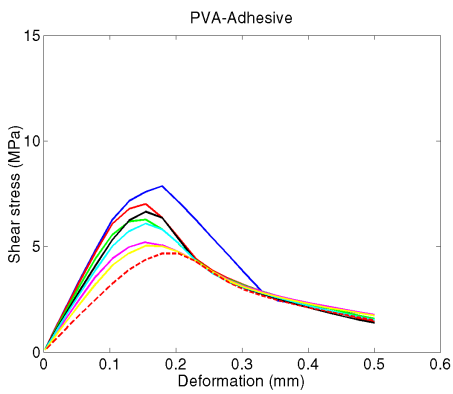

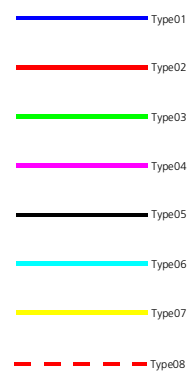

Stress distributions – EN302-1 – Type 01

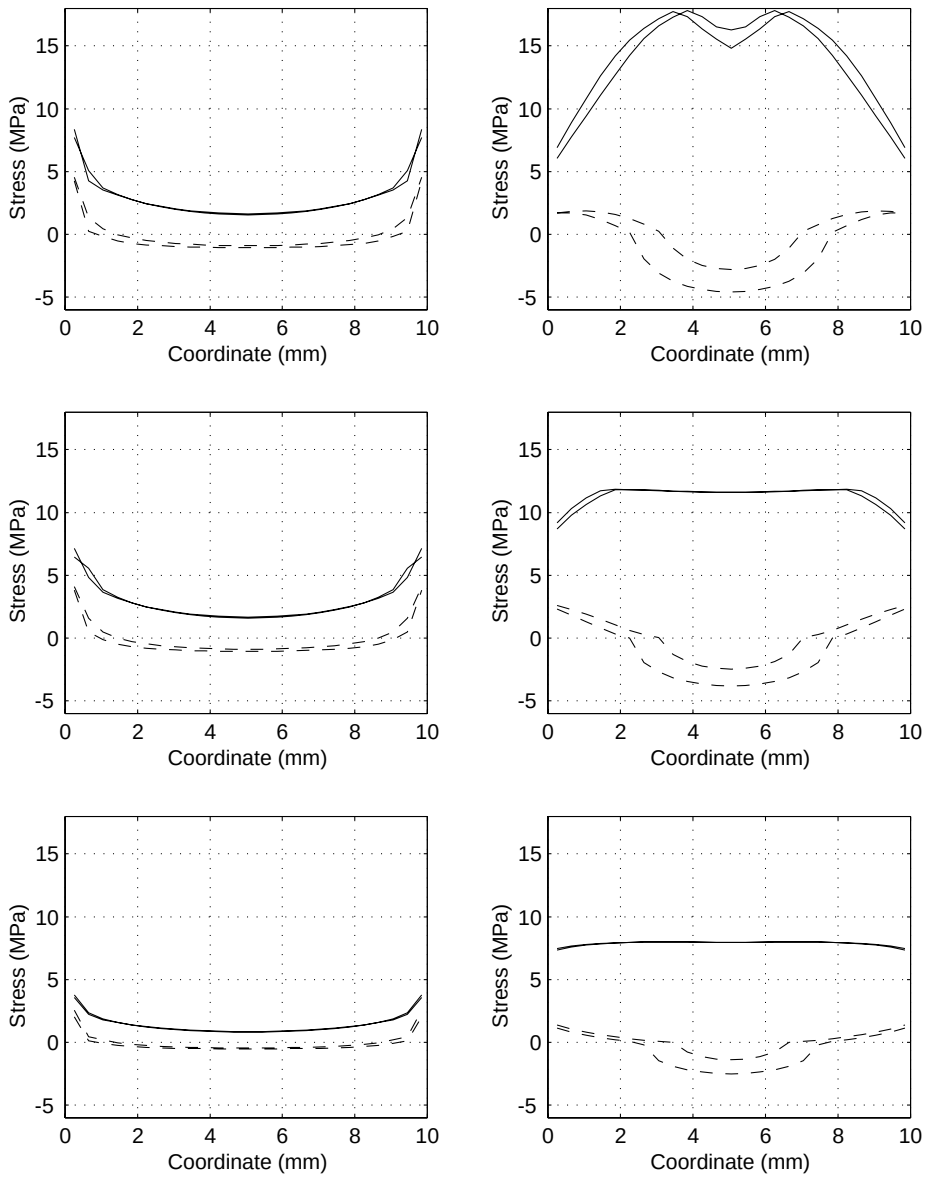

Figure 41 Linear elastic stress distributions (left) and stresses at maximum load (right). PRF (top) PUR (middle) and PVA (bottom). Solid lines are for shear stress and dashed for normal (peel) stress. The different curves are at the edge and in the centre respectively.

Stress distributions – EN302-1 – Type 02

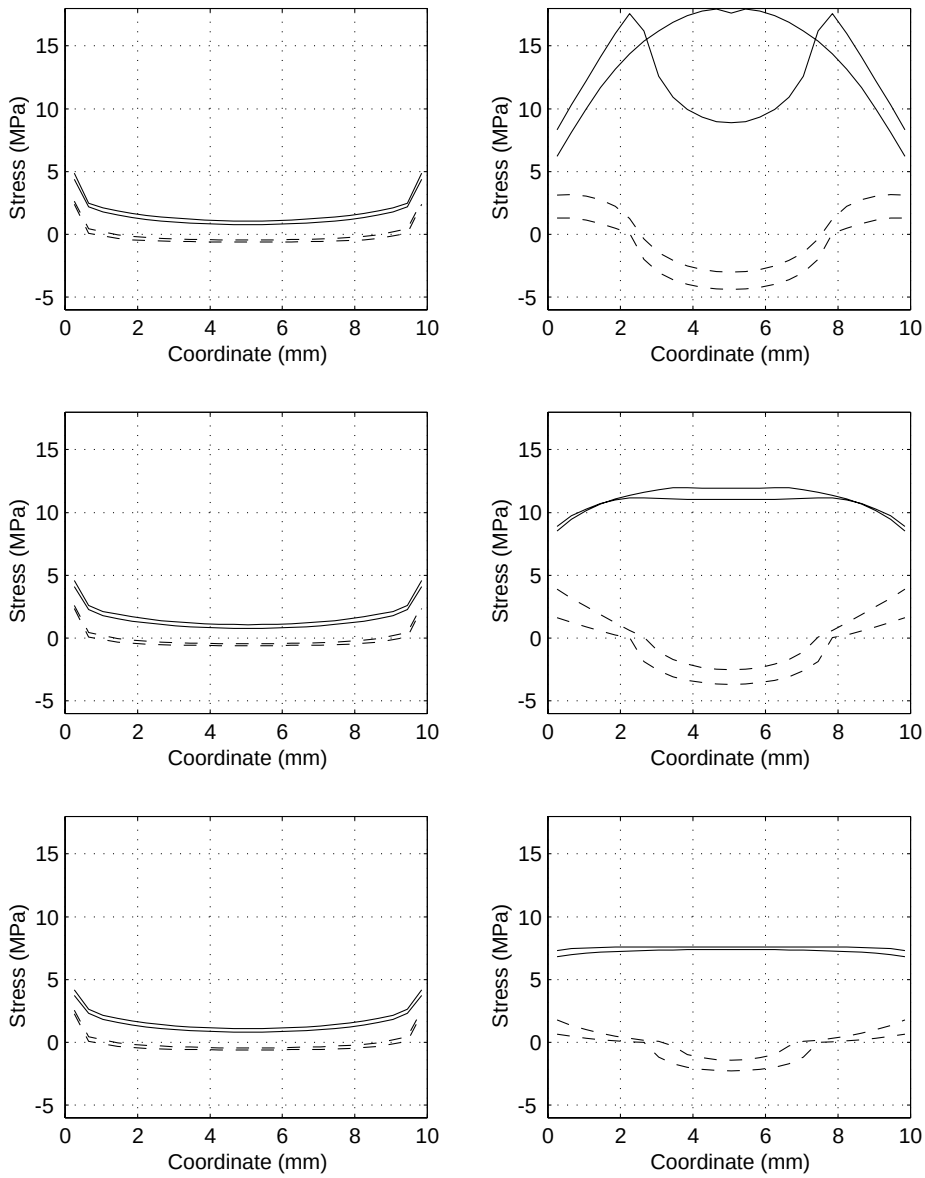

Figure 42 Linear elastic stress distributions (left) and stresses at maximum load (right). PRF (top) PUR (middle) and PVA (bottom). Solid lines are for shear stress and dashed for normal (peel) stress. The different curves are at the edge and in the centre respectively.

Stress distributions – EN302-1 – Type 03

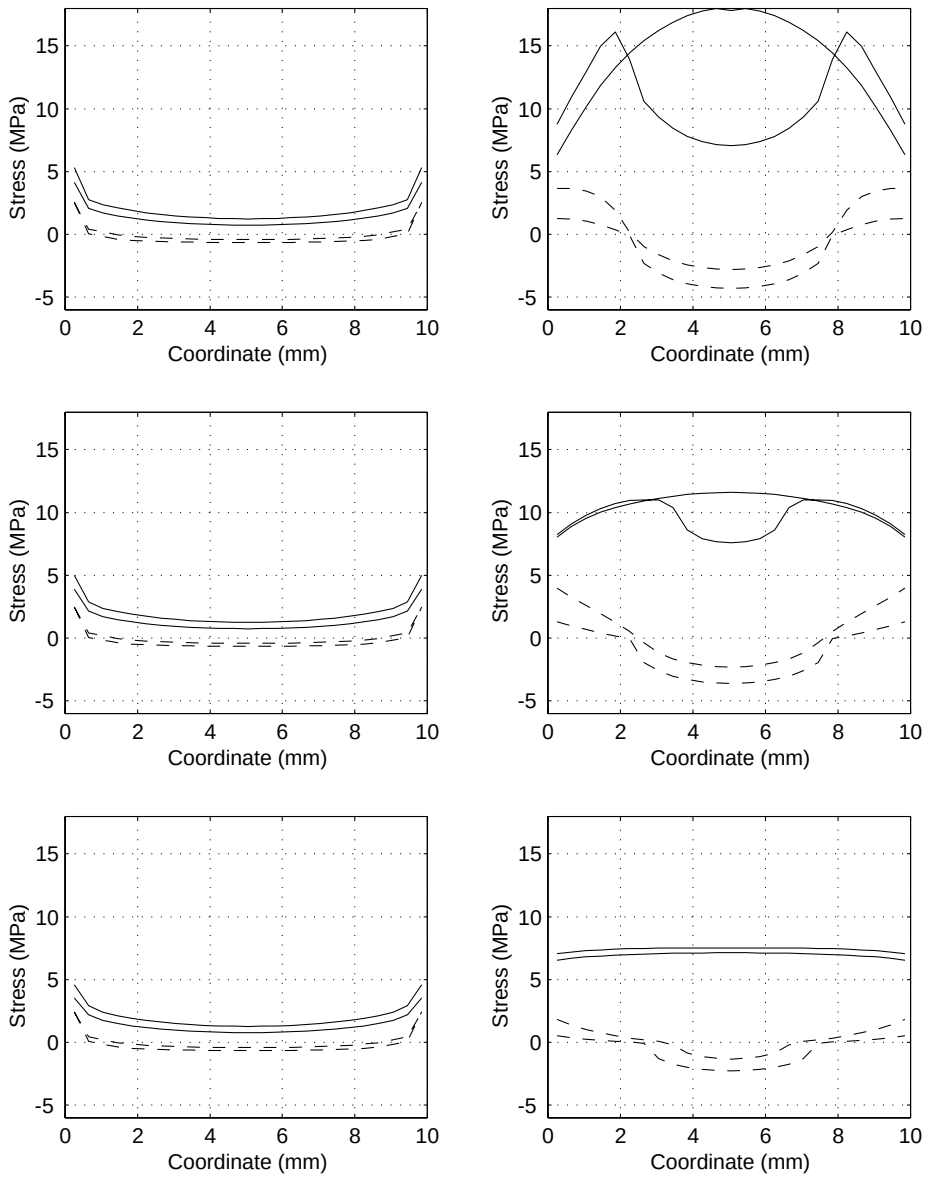

Figure 43 Linear elastic stress distributions (left) and stresses at maximum load (right). PRF (top) PUR (middle) and PVA (bottom). Solid lines are for shear stress and dashed for normal (peel) stress. The different curves are at the edge and in the centre respectively.

Stress distributions – EN302-1 – Type 04

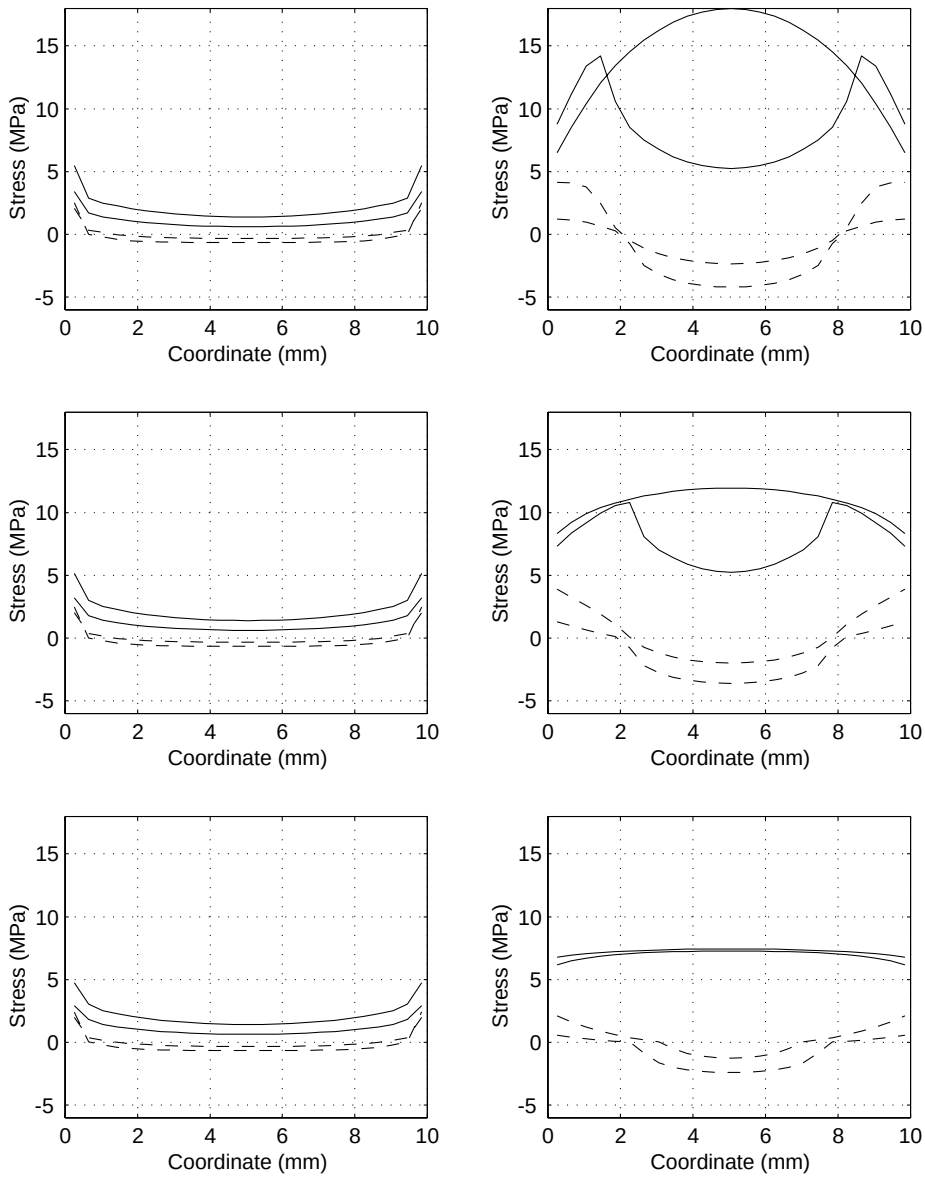

Figure 44 Linear elastic stress distributions (left) and stresses at maximum load (right). PRF (top) PUR (middle) and PVA (bottom). Solid lines are for shear stress and dashed for normal (peel) stress. The different curves are at the edge and in the centre respectively.

Stress distributions – EN302-1 – Type 05

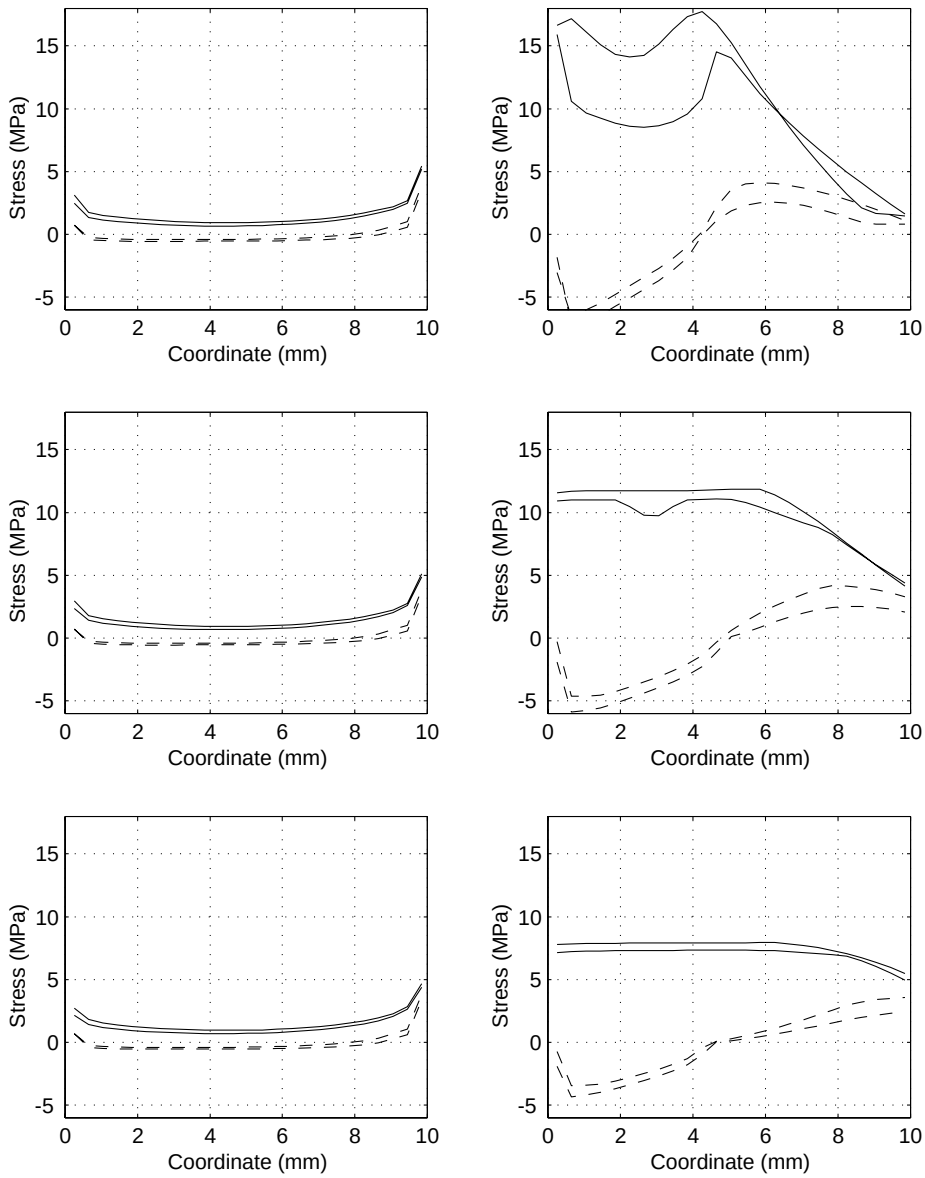

Figure 45 Linear elastic stress distributions (left) and stresses at maximum load (right). PRF (top) PUR (middle) and PVA (bottom). Solid lines are for shear stress and dashed for normal (peel) stress. The different curves are at the edge and in the centre respectively.

Stress distributions – EN302-1 – Type 06

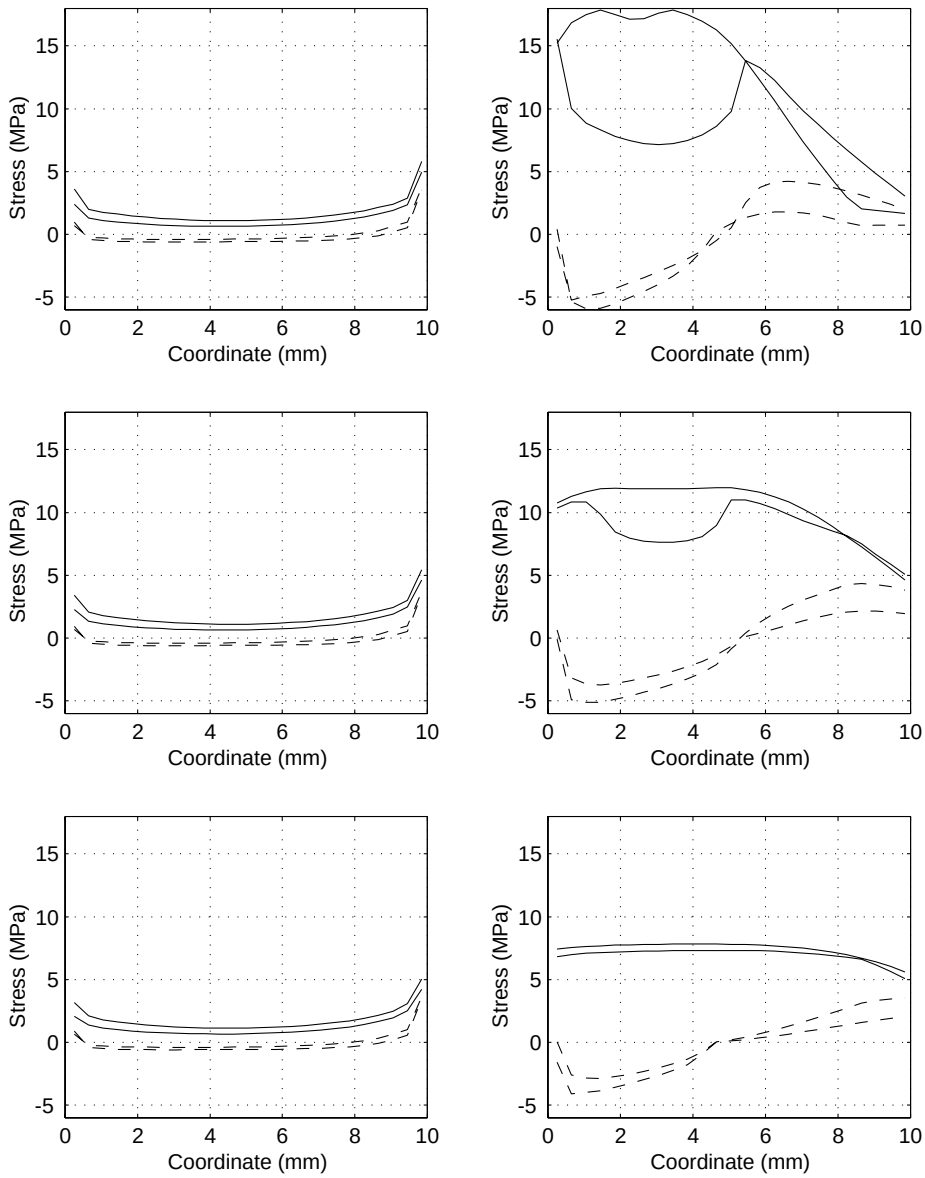

Figure 46 Linear elastic stress distributions (left) and stresses at maximum load (right). PRF (top) PUR (middle) and PVA (bottom). Solid lines are for shear stress and dashed for normal (peel) stress. The different curves are at the edge and in the centre respectively.

Stress distributions – EN302-1 – Type 07

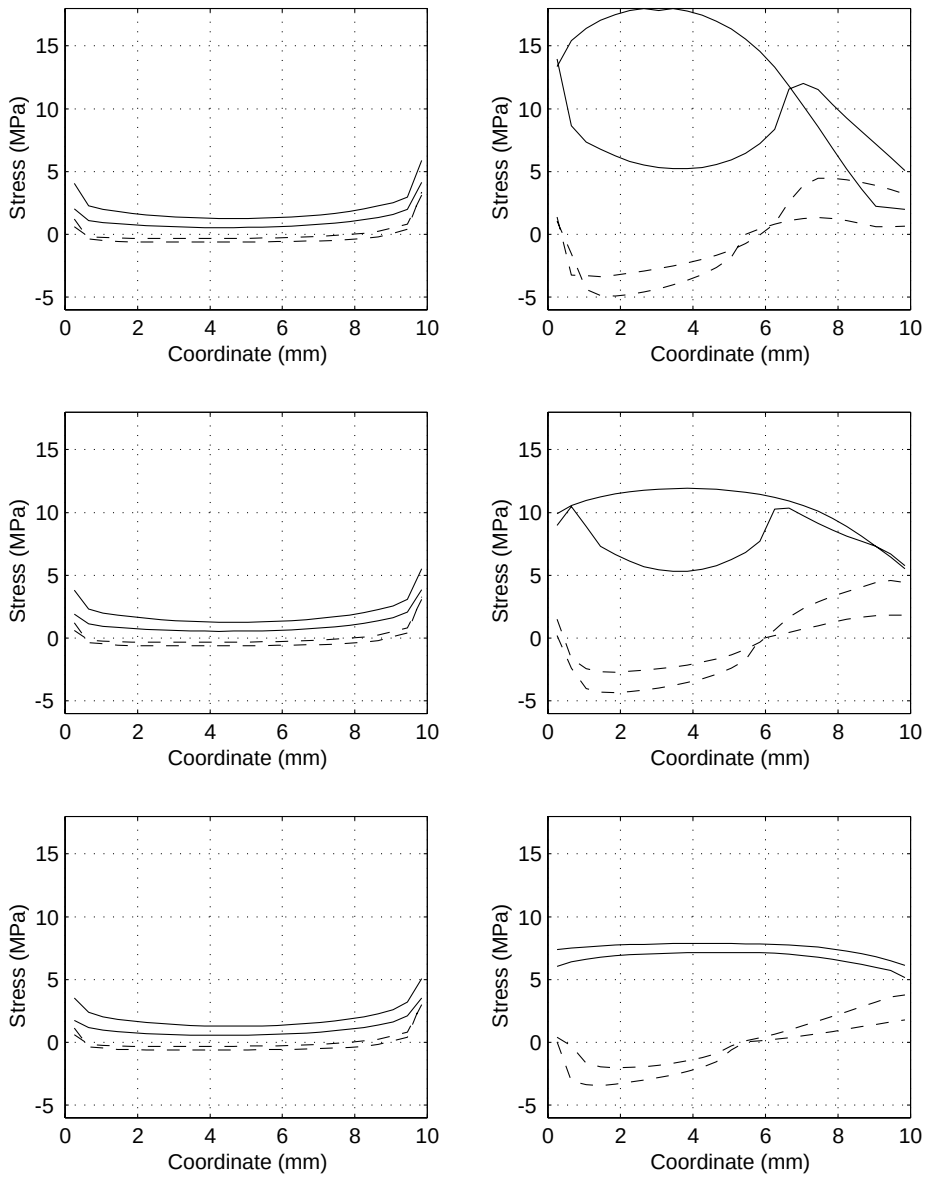

Figure 47 Linear elastic stress distributions (left) and stresses at maximum load (right). PRF (top) PUR (middle) and PVA (bottom). Solid lines are for shear stress and dashed for normal (peel) stress. The different curves are at the edge and in the centre respectively.

Stress distributions – EN302-1 – Type 08

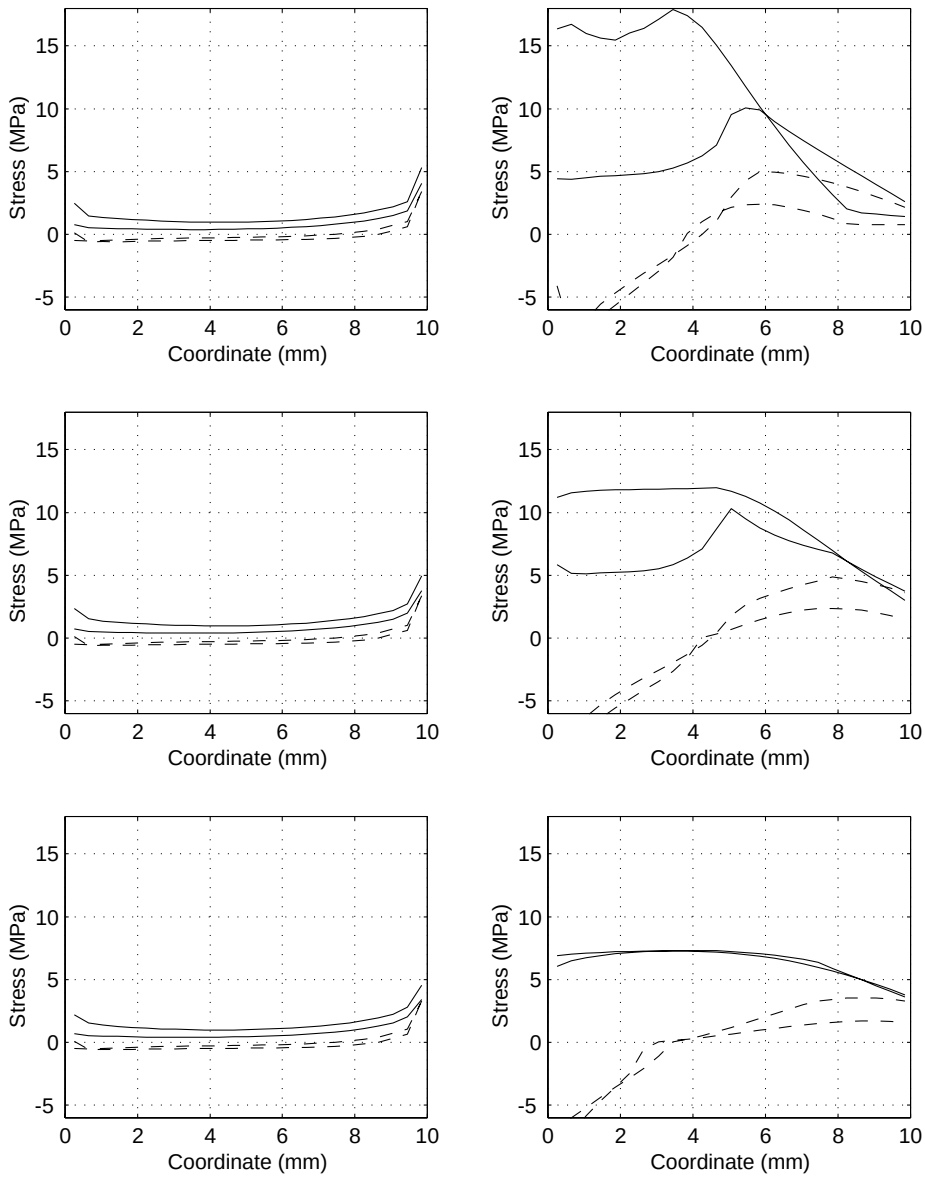

Figure 48 Linear elastic stress distributions (left) and stresses at maximum load (right). PRF (top) PUR (middle) and PVA (bottom). Solid lines are for shear stress and dashed for normal (peel) stress. The different curves are at the edge and in the centre respectively.

APPENDIX D: Detailed Results – ASTM D4680

Simulation Scheme and Results – ASTM D4680

Simulation type, no.	Eccentricity, e (mm)	Coefficient of friction	Slope of end-face
01	0	0.3	0
02	0.5	0.3	0
03	2	0.3	0
04	4	0.3	0
05	0	0	0
06	0	0.3	1°
07	0	0.3	5°

Name	P_{ult} (kN)[1]	τ (MPa)[2]	τ^* (-)[2]	τ (MPa)[3]	τ^* (-)[3]
PRF01	4.18	12.9	0.72	11.9	0.66
PUR01	3.94	12.2	1.02	11.2	0.93
PVA01	2.77	8.60	1.07	7.87	0.98
PRF02	3.87	12.0	0.67	11.5	0.64
PUR02	3.76	11.7	0.97	11.2	0.93
PVA02	2.66	8.24	1.03	7.89	0.99
PRF03	3.54	11.0	0.61	10.5	0.58
PUR03	3.68	11.4	0.95	10.9	0.91
PVA03	2.65	8.23	1.03	7.84	0.98
PRF04	3.08	9.56	0.53	9.02	0.50
PUR04	3.36	10.4	0.87	9.82	0.82
PVA04	2.65	8.21	1.03	7.74	0.97
PRF05	3.24	10.1	0.56	10.1	0.56
PUR05	3.29	10.2	0.85	10.2	0.85
PVA05	2.44	7.57	0.95	7.57	0.95
PRF06	2.74	8.49	0.47	6.66	0.37
PUR06	2.81	8.71	0.73	6.83	0.57
PVA06	2.42	7.50	0.94	5.84	0.73
PRF07	2.58	8.00	0.44	6.25	0.35
PUR07	2.63	8.17	0.68	6.36	0.53
PVA07	2.37	7.35	0.92	5.71	0.71

[1] The ultimate load for the symmetric *half*.
[2] The values are derived from global load divided by fracture area and include frictional forces
[3] "True stress values" i.e. the values are derived from the calculated stress distribution in the bond line.

Average shear stress versus deformation – ASTM D4680

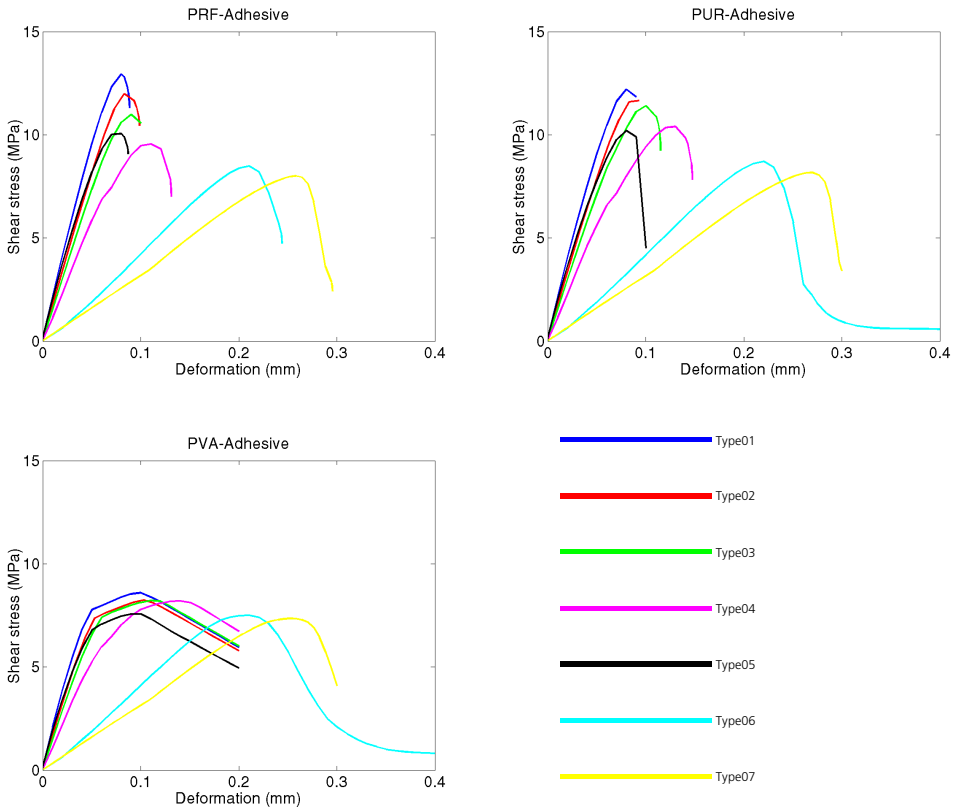

Stress distributions – ASTM D4680 – Type 01

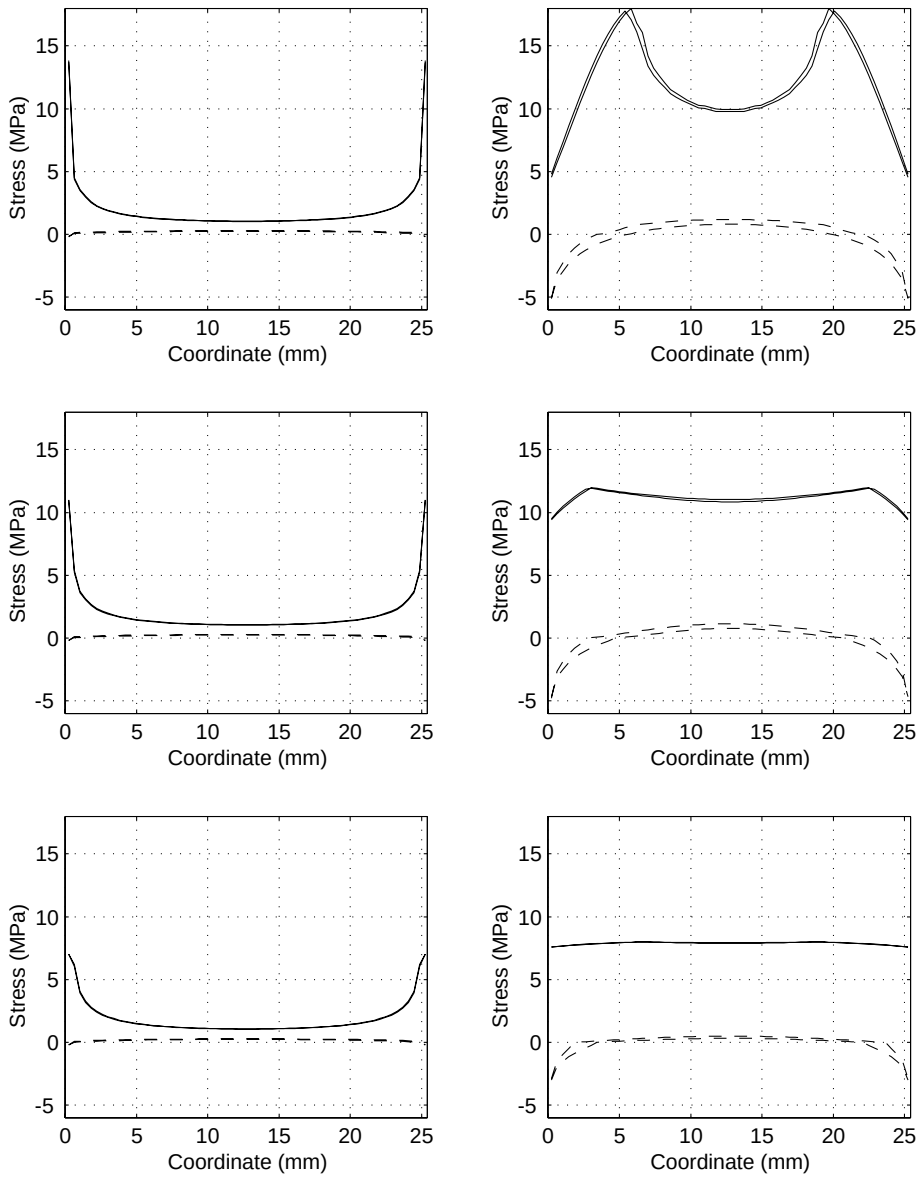

Figure 49. Linear elastic stress distributions (left) and stresses at maximum load (right). PRF (top) PUR (middle) and PVA (bottom). Solid lines are for shear stress and dashed for normal (peel) stress. The different curves are at the edge and in the centre respectively.

Stress distributions – ASTM D4680 – Type 02

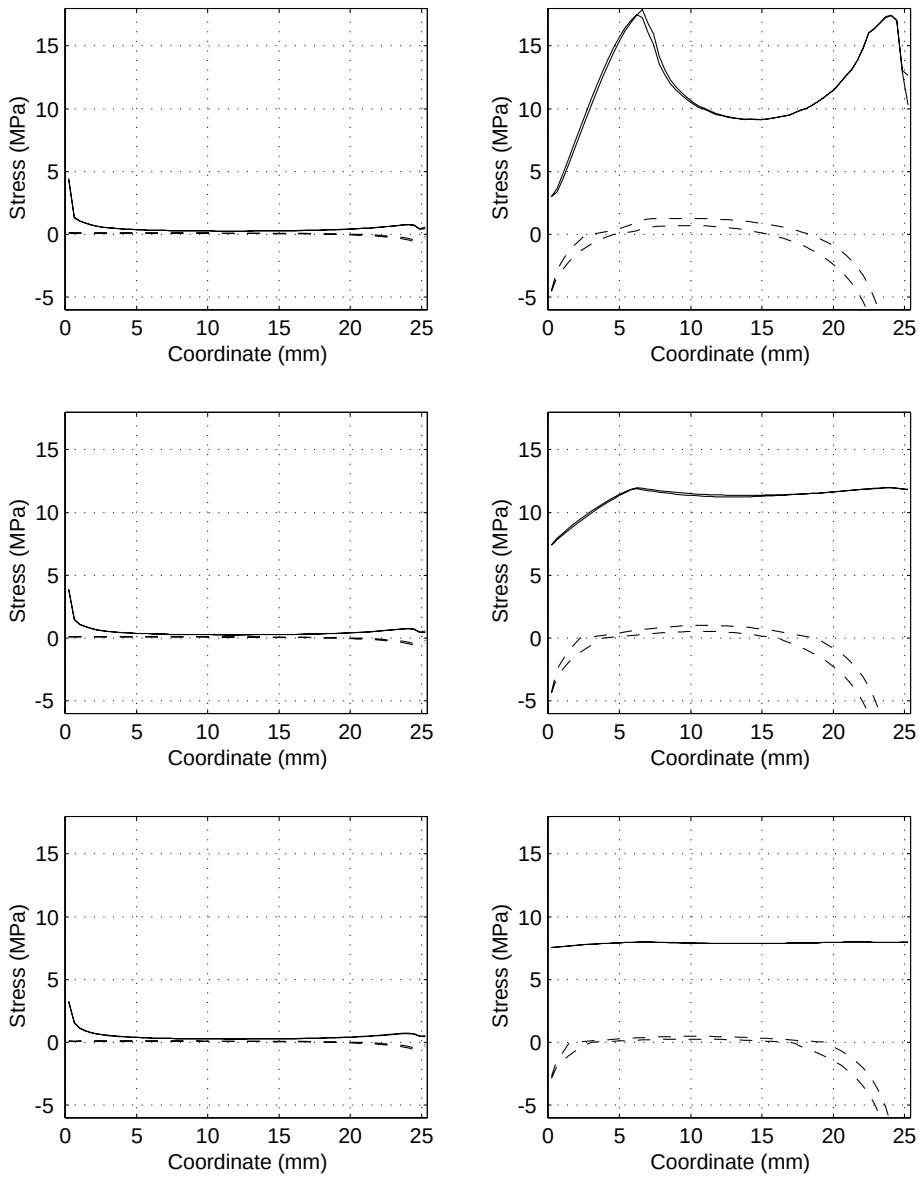

Figure 50. Linear elastic stress distributions (left) and stresses at maximum load (right). PRF (top) PUR (middle) and PVA (bottom). Solid lines are for shear stress and dashed for normal (peel) stress. The different curves are at the edge and in the centre respectively.

Stress distributions – ASTM D4680 – Type 03

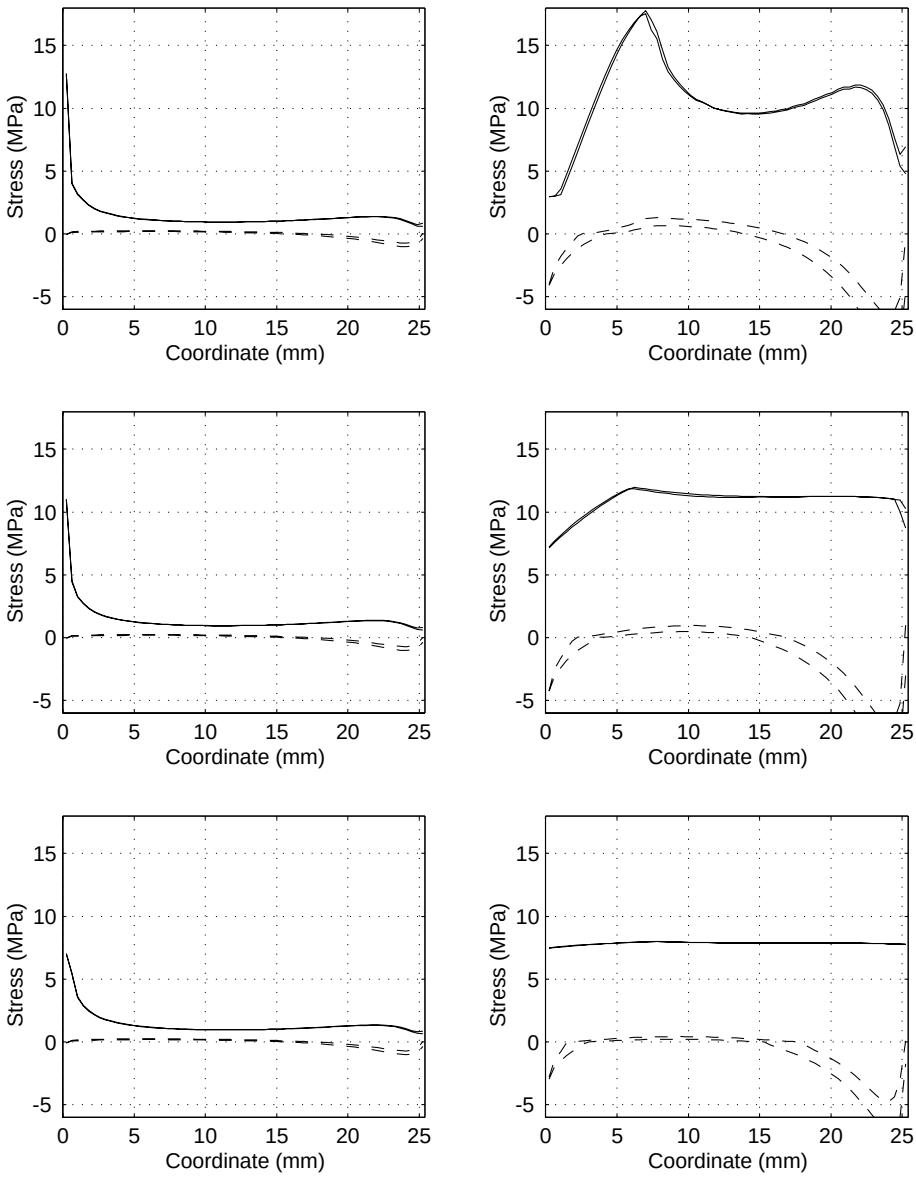

Figure 51. Linear elastic stress distributions (left) and stresses at maximum load (right). PRF (top) PUR (middle) and PVA (bottom). Solid lines are for shear stress and dashed for normal (peel) stress. The different curves are at the edge and in the centre respectively.

Stress distributions – ASTM D4680 – Type 04

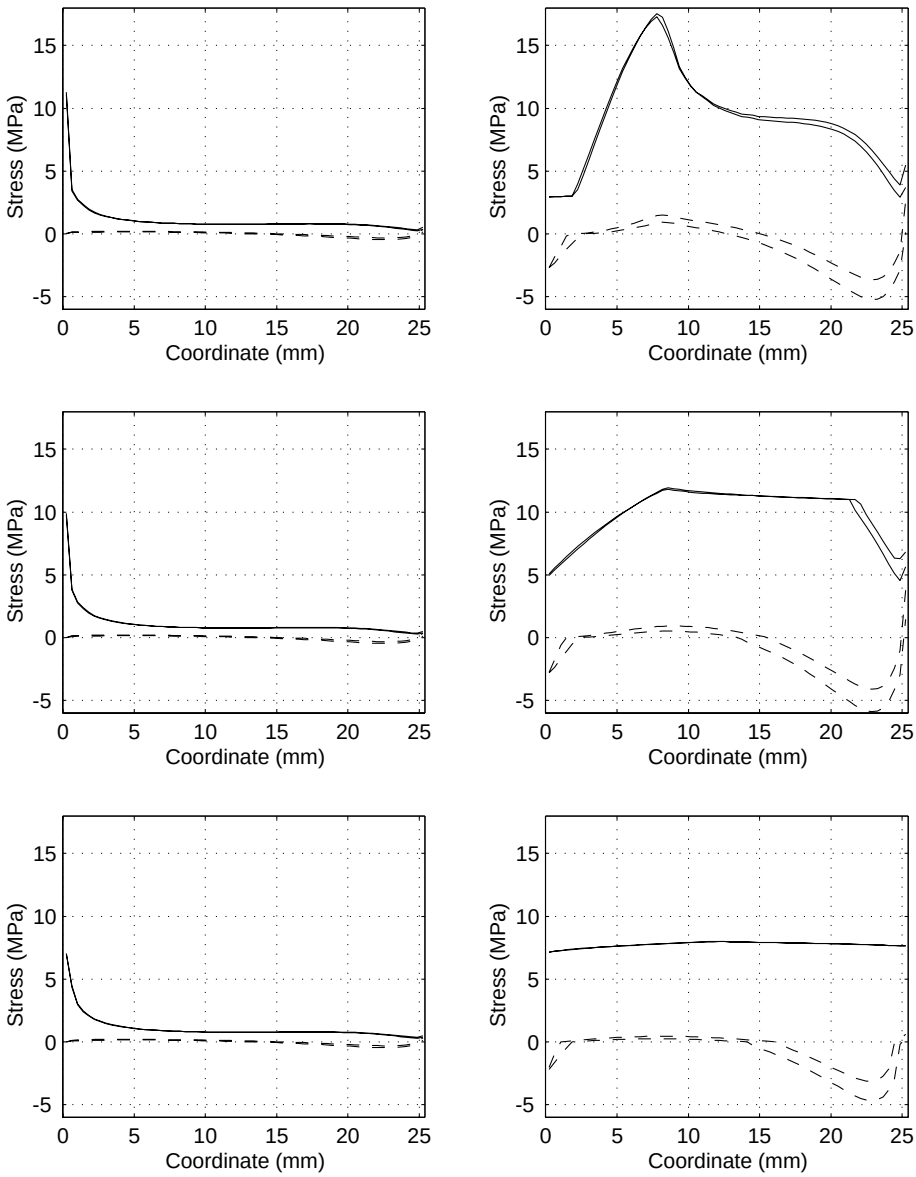

Figure 52. Linear elastic stress distributions (left) and stresses at maximum load (right). PRF (top) PUR (middle) and PVA (bottom). Solid lines are for shear stress and dashed for normal (peel) stress. The different curves are at the edge and in the centre respectively.

Stress distributions – ASTM D4680 – Type 05

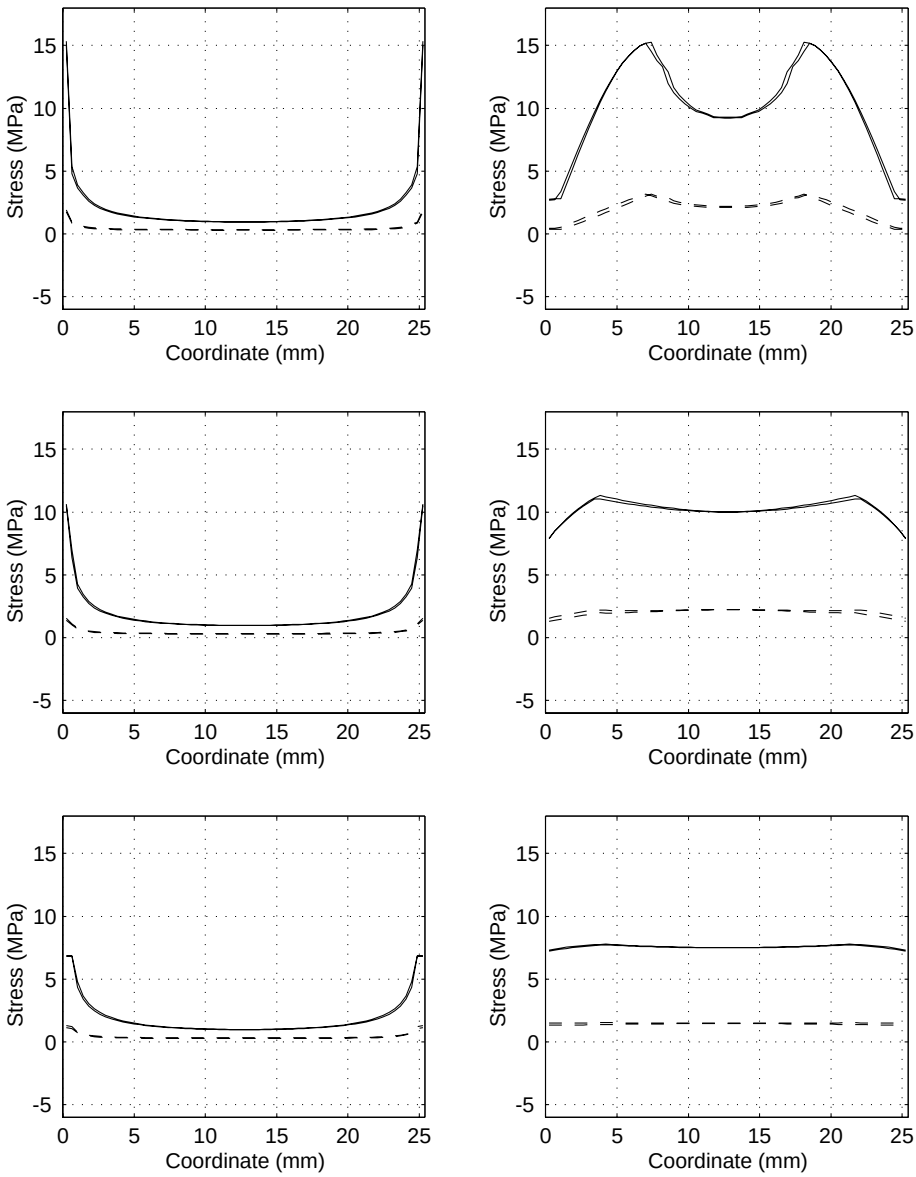

Figure 53. Linear elastic stress distributions (left) and stresses at maximum load (right). PRF (top) PUR (middle) and PVA (bottom). Solid lines are for shear stress and dashed for normal (peel) stress. The different curves are at the edge and in the centre respectively.

Stress distributions – ASTM D4680 – Type 06

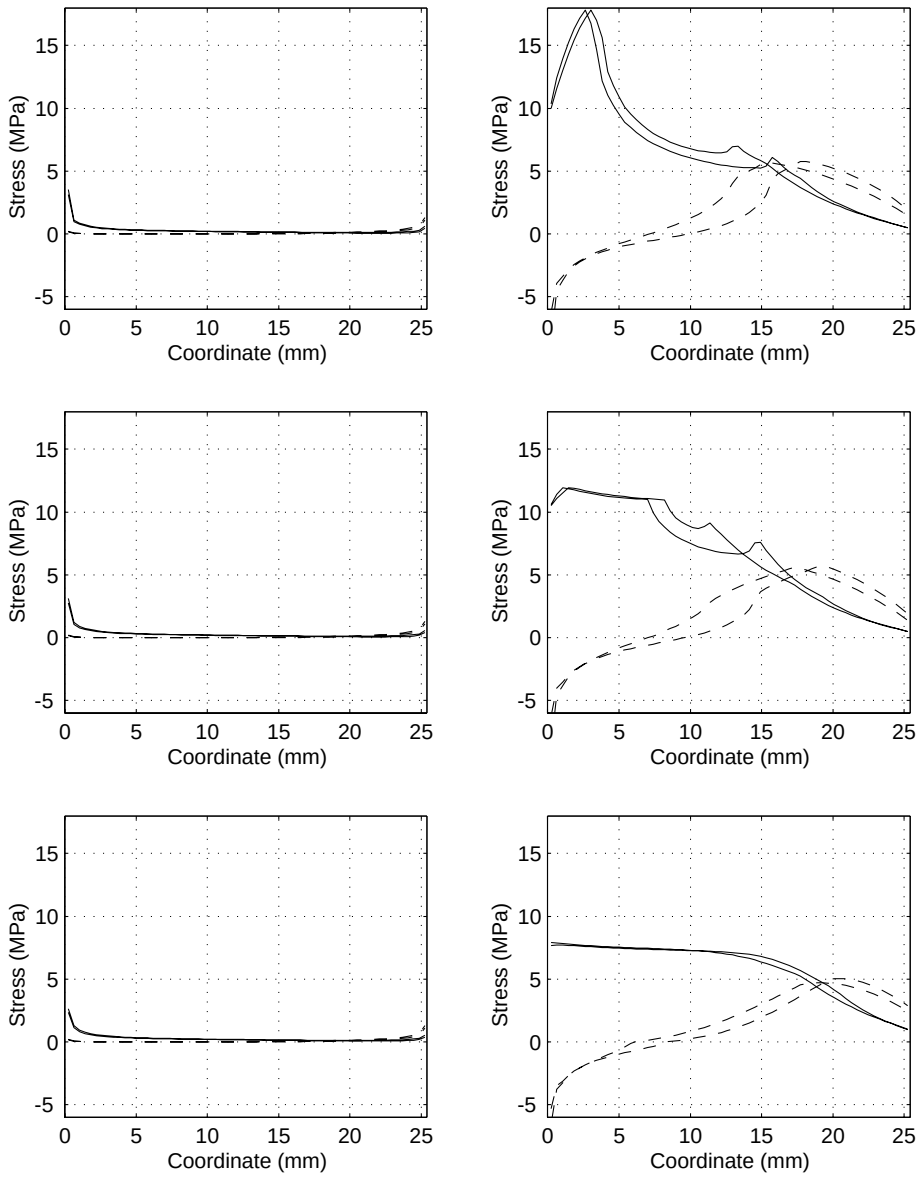

Figure 54. Linear elastic stress distributions (left) and stresses at maximum load (right). PRF (top) PUR (middle) and PVA (bottom). Solid lines are for shear stress and dashed for normal (peel) stress. The different curves are at the edge and in the centre respectively.

Stress distributions – ASTM D4680 – Type 07

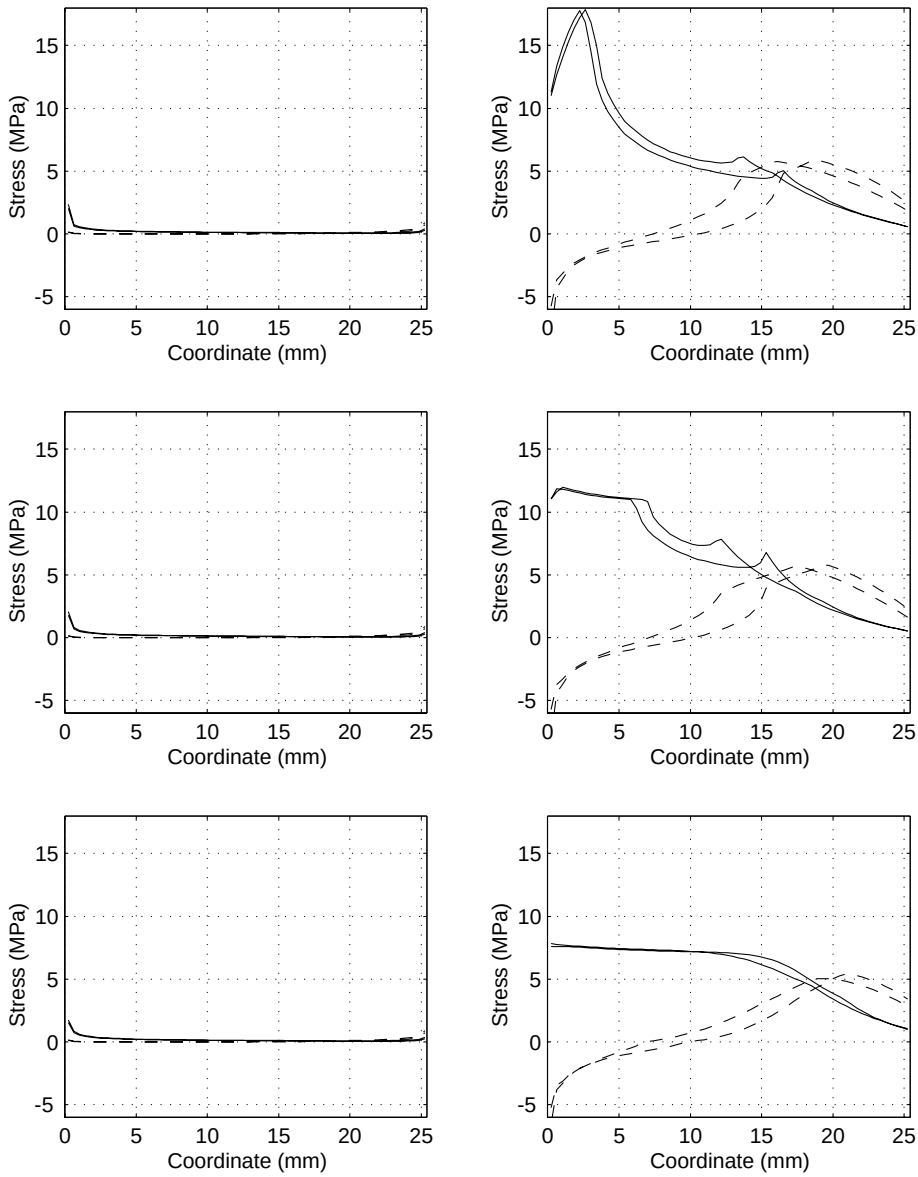

Figure 55. Linear elastic stress distributions (left) and stresses at maximum load (right). PRF (top) PUR (middle) and PVA (bottom). Solid lines are for shear stress and dashed for normal (peel) stress. The different curves are at the edge and in the centre respectively.